Acta Crystallographica Section A
Foundations of Crystallography
ISSN 0108-7673

Received 4 August 2006
Accepted 23 October 2006

Multiple twinning in cubic crystals: geometric/algebraic study and its application for the identification of the $\Sigma 3^n$ grain boundaries

Cyril Cayron

CEA-Grenoble DRT/LITEN/DTH, 17 rue des Martyrs, 38054 Grenoble, France. Correspondence e-mail: cyril.cayron@cea.fr

Multiple twinning in cubic crystals is represented geometrically by a three-dimensional fractal and algebraically by a groupoid. In this groupoid, the variant crystals are the objects, the misorientations between the variants are the operations, and the $\Sigma 3^n$ operators are the different types of operations (expressed by sets of equivalent operations). A general formula gives the number of variants and the number of $\Sigma 3^n$ operators for any twinning order. Different substructures of this groupoid (free group, semigroup) can be equivalently introduced to encode the operations with strings. For any coding substructure, the operators are expressed by sets of equivalent strings. The composition of two operators is determined without any matrix calculation by string concatenations. It is multivalued due to the groupoid structure. The composition table of the operators is used to identify the $\Sigma 3^n$ grain boundaries and to reconstruct the twin related domains in the electron back-scattered diffraction maps.

1. Introduction

'A twin is a complex crystalline edifice built up of two or more homogeneous parts of the same crystal species that are in contact and oriented with respect to each other according to well defined laws' (Friedel, 1904). The different origins of the twins (growth, recrystallization, mechanical deformation) are detailed by Hahn & Klapper (2003). In this paper, only the $\Sigma 3$ twins in cubic materials will be studied. These twins, also called in mineralogy sphalerite twins, spinel twins or diamond twins, belong to the class of 'twins by reticular merohedry' (Friedel, 1904), *i.e.* there is a partial but exact coincidence between the lattices of each individual crystal. $\Sigma 3$ means that this coincidence occurs only for one third of the lattices. More generally, two identical but misoriented cubic lattices have some points in coincidence that constitute a coincidence site lattice (CSL) if and only if they are linked by a transformation matrix T of the form

$$T = \frac{1}{\sum}\begin{bmatrix} a_{11} & a_{12} & a_{13} \\ a_{21} & a_{22} & a_{23} \\ a_{31} & a_{32} & a_{33} \end{bmatrix}, \qquad (1)$$

where a_{ij} are integers and Σ is the ratio of the unit volume of the CSL referred to the unit volume of the crystal lattice (Grimmer *et al.*, 1974; Grimmer, 1976). Very often in metallurgy, metals with low stacking-fault energy form twins by annealing and recrystallization (Kronberg & Wilson, 1949; Kopezky *et al.*, 1991). In this case, a crystal, which we will call the primary crystal, can form twins (twins of first generation), which can themselves form twins (twins of second generation), and so on. Each crystal in this assembly is linked to another by a transformation matrix T with an associated $\Sigma = 3^n$ with $n \in \mathbb{N}$. These crystals are connected by a chain of $\Sigma 3$ twins (*i.e.* by $\Sigma 3^n$ operators) and form a microstructural entity usually referred to as a twin-related domain (TRD) (Reed & Kumar, 2006).

Grain design engineering is an idea introduced by Watanabe (1985). It suggests that microstructures with a high fraction of 'special' grain boundaries (which can be obtained by optimizing the elaboration process or the thermo-mechanical treatments) have better mechanical properties, such as improved corrosion resistance, creep resistance or weldability. Since the special $\Sigma 3$ grain boundaries are considered to be the 'strongest' ones, many engineers are trying to create microstructures that have a high density of $\Sigma 3$ grain boundaries and large TRDs (Kumar *et al.*, 2000). These multiply twinned materials can be characterized using electron back-scatter diffraction (EBSD[1]) in a scanning electron microscope (SEM) (for examples, see Randle & Brown, 1989; Kumar *et al.*, 2000; Gertsman & Henager, 2003). Although the $\Sigma 3^n$ grain boundaries are easy to identify for $n \leq 4$, there is no

[1] The reader may refer to Schwartz *et al.* (2000) for an overview of the EBSD technique.

method that can automatically identify them for higher twinning orders. Indeed, the distribution of the orientations of multiply twinned crystals is very dense and nearly isotropic for $n \geq 5$, and consequently it is very difficult to distinguish a random misorientation from a special $\Sigma 3^n$ [this has been shown by Wilbrandt (1980) and will be discussed in detail later]. A similar problem has been encountered for phase-transformed materials during the identification of the operators and the reconstruction of parent grains from the EBSD data obtained from the daughter grains. A solution has been proposed by Cayron *et al.* (2006) based on groupoid composition tables introduced in Cayron (2006). However, a phase transition corresponds to only half a cycle and we need to generalize the theory to cycled-transformed materials. This paper is a geometric/algebraic study on the particular type of series of cycles of transformations known as multiple twinning.[2] The theoretical results allow the identification of the $\Sigma 3^n$ grain boundaries and the reconstruction of the TRDs encountered in some metallurgical problems.

In §2, the approach of Reed *et al.* (2004) on multiple twinning in metallurgy is discussed. A simple introduction to groupoids is given in §3 so as to facilitate the understanding of the further sections. In §4, multiple twinning is represented geometrically by a three-dimensional fractal and algebraically by a groupoid. It is shown that the $\Sigma 3^\omega$ free group introduced by Reed *et al.* (2004) is a possible substructure of this groupoid. Another equivalent but not isomorphic substructure, the $\Sigma 3^\xi$ semigroup, is introduced in §5. In §6, the $\Sigma 3^n$ operators are encoded by sets of equivalent strings, and a general method to determine their composition is proposed. We prove that the composition is multivalued. The composition table (called groupoid composition table) is given for twinning orders up to $n = 4$. Finally, in §7, we study some engineering cases (local crystallographic environment of voids or hillocks in copper films, reconstruction of the TRDs in narrow copper lines) in order to show how this table can be used to identify the $\Sigma 3^n$ grain boundaries in some EBSD maps.

To begin, we must explain some notations. The point group $\mathbf{G}$ of a crystal will be considered as the group of matrices representing its orientational symmetries. $|\mathbf{G}|$ is the cardinality of the group $\mathbf{G}$ (*i.e.* the number of matrices). If $\mathbf{H}$ is a subgroup of $\mathbf{G}$, the expression $g\mathbf{H}$ means a left coset of matrices based on the subgroup $\mathbf{H}$, it is the set $\{gh, h \in \mathbf{H}\}$. The expression $\mathbf{G}T\mathbf{G}$, where T is a matrix, is the set $\{g_i T g_j, (g_i, g_j) \in \mathbf{G}^2\}$.

2. The different algebraic approaches of simple and multiple twinning

Theoretically, the first crystallographic studies on textures generated by multiple twinning date back to the 1940s (Kronberg & Wilson, 1949; Wilbrandt, 1980; Gottstein, 1984). Many authors briefly mention that the algebraic structure associated with multiple twinning is a group. However, this group is rarely defined completely and its properties are not always demonstrated. Its definition appears to vary in different publications. When no detail is given, it can be assumed that that group is $O(3)$ (the group of orthogonal matrices), but it could be also the subgroup constituted by all the matrices verifying equation (1), or a subgroup of this last group defined by imposing the condition $\Sigma = 3^n$. However, these groups are too large and do not represent the true nature of multiple twinning. In fact, in these groups two equivalent transformation matrices, corresponding to the same misorientation between two crystals but differing due to a different choice of bases in those crystals, would be treated as two distinct elements whereas it would be more appropriate to consider them as the same element.

2.1. The approach of Reed *et al.* (2004) to multiple twinning

An impressive study has recently been published by Reed *et al.* (2004) on how multiply twinned structures, and more generally the $\Sigma X^m \Sigma Y^n$ structures with X and Y integers, can be constructed from algebraic manipulations on quaternions, simplified by a string representation and illustrated using network graphs. This theoretical work has been recently summarized and applied to simulate multiply twinned microstructures (Reed & Kumar, 2006). Since we will often refer to this work, we will give a brief description of the part of their approach that deals with multiple twinning. The misorientation *from* a crystal 1 *to* a homophase crystal 2 can be expressed by a set of equivalent matrices $\mathbf{G}R_{12}\mathbf{G}$, where $R_{12} = R_1^{-1}R_2$ is a rotation from crystal 1 to crystal 2 and $\mathbf{G}$ is the point group of the cubic crystals. This set is called a 'subtype' and the order of the crystals in the pair $(1, 2)$ is important. The misorientation *between* two crystals 1 and 2 is expressed by a set of equivalent matrices $\mathbf{G}R_{12}\mathbf{G} \cup \mathbf{G}R_{21}\mathbf{G}$, with $R_{21} = R_{12}^{-1}$. This set is called a 'type' and the order of the crystals in the pair (1, 2) is not important. The 'types' define matrices that are 'cubically' equivalent.[3] In their paper, Reed *et al.* (2004) have used the 'types' and the corresponding sets of equivalent quaternions. For example, $\Sigma 3$ is a 'type' and the set contains the quaternions of shape [0111], [0112] and [3111]. From the set of equivalent quaternions, the authors have separated four 'cosets' which contains the quaternions [0111], $[0\bar{1}\bar{1}1]$, $[01\bar{1}\bar{1}]$ and $[0\bar{1}1\bar{1}]$, and correspond to the 180° rotations with [111], $[1\bar{1}\bar{1}]$, $[\bar{1}\bar{1}1]$ and $[\bar{1}1\bar{1}]$ axes, respectively. Each 'coset' was then called a, b, c and d (in Reed & Kumar, 2006), and each $\Sigma 3^n$ operation was expressed by a string constituted of these four

[2] Multiple twinning can be imagined as repeated transformations (see §4).

[3] The notion of 'cubical equivalence' was introduced by Grimmer (1974) who studied the matrix and quaternion expressions of the misorientation between two cubic crystals. However, as already pointed out by Reed *et al.* (2004), it is in general possible to distinguish the misorientation from crystal 1 to crystal 2 and the misorientation from crystal 2 to crystal 1. The two subtypes are then complementary polar subtypes (see §2.2). Thus, the subtypes contain more information than the types and, in this paper, we will use the notion of subtype. We will say that two matrices T_x and T_y are 'polarly cubically equivalent' if and only if they belong to the same subtype, *i.e.* they form the same set of matrices $\mathbf{G}T_x\mathbf{G} = \mathbf{G}T_y\mathbf{G}$, with $\mathbf{G}$ the point group of the cubic crystals (sometimes denoted $\Sigma 1$).

letters. The strings can be composed using simple concatenation and by taking into consideration a rule that eliminates the pairs of equal consecutive letters (for example *abbcd* = *acd*). All the operations can be represented by a graph. With this representation, the set of the $\Sigma 3^n$ operations form a free group[4] called $\Sigma 3^\omega$. The work of Reed *et al.* (2004) brings a new understanding to multiple twinning and introduces a rule on the Σ numbers that can help metallurgists to analyse structures with $\Sigma 3^n$ grain boundaries. However, many questions can be raised. The decomposition of the set of equivalent quaternions into four cosets is not clearly explained. It is intuitive (because the [111], $[1\bar{1}\bar{1}]$, $[\bar{1}\bar{1}1]$ and $[\bar{1}1\bar{1}]$ axes are equivalent), but what are the algebraic justifications for this decomposition? Are the cosets left or right? What is the subgroup on which they are based? The authors assume that a representative can be 'arbitrarily' chosen in the cosets, and they have built the group $\Sigma 3^\omega$, not with the entire cosets but with the four quaternions $a = [0111]$, $b = [0\bar{1}\bar{1}1]$, $c = [01\bar{1}\bar{1}]$ and $d = [0\bar{1}1\bar{1}]$. What could be the structure if other representatives were considered? Would we obtain the same group with the same elimination rule? There are also other limitations discussed by the authors, such as 'without cubic symmetry, the natural mapping between integer quaternions and CSL rotations is lost'. Is it possible to introduce another approach without quaternions (which could therefore be applied to non-cubic materials)? Moreover, because the four elements *a*, *b*, *c*, *d* generate an infinity of new operations, the group $\Sigma 3^\omega$ is infinite. Why is it not possible to build a finite algebraic structure to describe finite cases such as the one of a crystal and its four twinned variants? A last but not least question is also raised: we know that the composition of two $\Sigma 3$ operators produces either a $\Sigma 1$ operator or a $\Sigma 9$ operator. However, in a group the composition is a 'classical' mathematical application (the composition of two elements gives only one element), so a group structure cannot explain *the multivalued aspect* of the composition of the $\Sigma 3^n$ operators. What could be the algebraic structure describing the multiple twinning and its multivalued composition? We will try to answer these questions in this paper.

2.2. A brief overview on simple twinning

The work of Reed *et al.* (2004) is mainly based on metallurgical tools (such as the CSL rotations). The crystallographic developments of twinning applied in other fields of material science can be used advantageously to complete their approach. The colour group introduced by Shubnikov & Koptsik (1974) (see also Senechal, 1983) is now integrated in the modern theories of twinning. Crystallographers working in mineralogy (Wadhawan, 1997; Hahn & Klapper, 2003) and those working in physics of ferroelectric domains (Janovec, 1976) have made a synthesis of their respective approaches. This synthesis uses mathematical tools based on modern group theory such as orbits, stabilisers, coset partitioning *etc.* (Hahn *et al.*, 1999; Janovec *et al.*, 2003). Some crystallographers interested in grain boundaries are following the work of Pond & Vlachavas (1983) and are trying to integrate the CSL rotations in that synthesis (Grimmer & Nespolo, 2006).

Let us briefly explain the principle of coset partitioning in the case of twinning. We call $\mathbf{G}_0$ the point group of crystal 0 and T a twin operation. We call $\mathbf{G}_1$ the point group of crystal 1 which is the twin of crystal 0 by the operation T. If the matrices that constitute $\mathbf{G}_1$ are expressed in the same base as those of $\mathbf{G}_0$, the two groups are linked by $\mathbf{G}_1 = T\mathbf{G}_0T^{-1}$. The two crystals have some symmetries in common that constitute the intersection group $\mathbf{H} = \mathbf{G}_0 \cap \mathbf{G}_1$. Moreover, owing to the symmetries of the crystal 0, more than one twin crystal might be created and each element g of $\mathbf{G}_0$ that does not belong to $\mathbf{H}$ creates a new variant. Thus the group $\mathbf{G}_0$ can be partitioned into left cosets that represent the distinct variants:

$$\mathbf{G}_0 = g_0\mathbf{H} \cup g_2\mathbf{H} \cup \ldots \cup g_{N-1}\mathbf{H} \qquad (2)$$

with $g_0 = e$ the neutral element (*i.e.* the identity matrix). The number of variants is given by the Lagrange formula $N = |\mathbf{G}_0|/|\mathbf{H}|$ and their orientations are given by the sets $g_i\mathbf{H}T$. Now, we can explain the idea of Reed *et al.* (2004), the 'cosets' of their decomposition are in fact the sets of type $g_i\mathbf{H}T$ (which are not strictly speaking cosets because only $g_i\mathbf{H}$ are cosets).

The set of cosets in the decomposition (2) represents the assembly of twinned variants. This is sometimes called 'the reduced composite group'. However, this name may be confusing. One must distinguish the group $\mathbf{G}_0$ of crystal 0 that has generated the set of variants from the set of variants itself (*i.e.* the set of cosets) given by

$$\mathbf{G}_0/\mathbf{H} = \{g_0\mathbf{H}, g_1\mathbf{H}, \ldots, g_{N-1}\mathbf{H}\}. \qquad (3)$$

In general, $\mathbf{G}_0/\mathbf{H}$ does not have a group structure. *It is a group if and only if* $\boldsymbol{H}$ *is a normal subgroup of* $\boldsymbol{G}_0$. If this condition is fulfilled, $\mathbf{G}_0/\mathbf{H}$ is a group and each coset of this group can be represented by one matrix arbitrarily chosen in each coset. For example, $\mathbf{H}$ is a normal subgroup when there are only two cosets in the set (3). However, we stress here that *the condition of normality of* $\boldsymbol{H}$ *is not fulfilled in the case of* $\Sigma 3$ *twinning* as discussed in Cayron (2006). Consequently, although one matrix (or one quaternion) can be arbitrarily chosen in each coset for numerical calculations (Reed *et al.*, 2004), a method based on arbitrary choices of representatives cannot be used to justify the algebraic structure of multiple twinning.

The misorientations from a variant represented by the coset $g_i\mathbf{H}$ to a variant represented by the coset $g_j\mathbf{H}$ are isomorphic to the double cosets $\mathbf{H}g_{ij}\mathbf{H}$, where $g_{ij} = g_i^{-1}g_j$ (Janovec *et al.*, 2003; Cayron, 2006). Therefore, the distinct types of misorientations between ordered pairs of variants are given by the partition of $\mathbf{G}_0$ into double cosets,

$$\mathbf{G}_0 = \mathbf{H}g_0'\mathbf{H} \cup \mathbf{H}g_2'\mathbf{H} \cup \ldots \cup \mathbf{H}g_{N^0-1}'\mathbf{H}. \qquad (4)$$

These types of misorientations are also the orbits of the action of $\mathbf{G}$ on the sets of the ordered pairs of variants (Janovec,

[4] If $\mathbf{S}$ is a set, the expressions $s_1^{\varepsilon_1} \ldots s_n^{\varepsilon_n}$ with $s_i \in \mathbf{S}$ and $\varepsilon_i \in \{-1, 1\}$ are called the strings (or words) of $\mathbf{S}$. A string is said to be reduced if it does not contain two adjacent terms of the form $s_i^1 s_i^{-1}$ or $s_i^{-1}s_i^1$. A free group $\mathbf{F}$ is a group generated by a set $\mathbf{S}$ in which the distinct elements are represented by distinct reduced strings in $\mathbf{S}$.

1972). Double cosets are not limited to crystallography; they are also widely used in physics and chemistry[5] (Ruch & Klein, 1983). Since double cosets can be viewed as types of actions that act on the variants, we call them *operators*. Their set is written

$$\mathbf{H}\backslash\mathbf{G}_0/\mathbf{H} = \{\mathbf{H}g'_0\mathbf{H}, \mathbf{H}g'_2\mathbf{H}, \ldots, \mathbf{H}g'_{N^0-1}\mathbf{H}\}. \quad (5)$$

The primes in g'_i are introduced to distinguish the elements g'_i of (5) from the elements g_i of (3). The number of operators, N^0, is given by the Burnside formula or it can be obtained by a class equation (Cayron, 2006). In general, it is possible to distinguish the operator transforming the variant i into the variant j from the operator transforming the variant j into the variant i because in general $\mathbf{H}g_{ij}\mathbf{H}$ and $\mathbf{H}g_{ij}^{-1}\mathbf{H}$ are two distinct double cosets. The operators are then called *polar*. If it is not the case, *i.e.* $\mathbf{H}g_{ij}\mathbf{H} = \mathbf{H}g_{ij}^{-1}\mathbf{H}$, the operators are called *ambivalent* (Janovec & Přívratská, 2003). Now, it can be realized that the 'subtypes' (see §2.1) correspond to the operators, and that the 'types' correspond to an 'artificially forced' union of complementary operators $\mathbf{H}g_{ij}\mathbf{H} \cup \mathbf{H}g_{ij}^{-1}\mathbf{H}$ (always ambivalent).

In Cayron (2006), all these ideas have been used to show that the set of variants associated with the set of operations that link them form an algebraic structure called groupoid of orientational variants. Is it possible to generalize the concept of groupoid to multiply twinned variants? Before going further, we would like to give some explanations on groupoids and a possible way to use them in crystallography.

3. A brief introduction to groupoids and operators

Groupoids are very useful because they are 'the ideal tool for describing symmetries that apply only to parts of systems. Groupoids are more flexible and often more appropriate than the better-known groups ...' (Stewart, 2004). Groupoids were first introduced in mathematics by Brandt (1926) and they now play a key role in the category and homotopy theories. For an exact definition and mathematical details, the reader may refer to Brown (1987) or Weinstein (1996). Groupoids were used in material science to represent polytypic structures, also known as order–disorder structures (Dornberger-Schiff & Grell-Niemann, 1961; Sadanaga, 1978; Fichtner, 1986). Their practical applications however have remained mainly limited to the problem of diffraction enhancement of symmetry (Sadanaga & Ohsumi, 1979). Since the definition of groupoids given by mathematicians may be difficult to understand for non-mathematicians, we would like to give here our personal geometrical and simple vision on this algebraic structure.

The most important point to understand is the groupoid composition law. It says that two pairs of objects (i, j) and (j, k) can be composed and the result is (i, k). This condition is classical and everyone has used it to add geometrically two vectors **U** and **V**. Each vector is written as a pair of points such that $\mathbf{U} = (P_1, P_2)$, $\mathbf{V} = (P_2, P_3)$ and the result is $\mathbf{W} = \mathbf{U} + \mathbf{V} = (P_1, P_3)$. Such geometrical construction has been forgotten in Cartesian geometry because the addition of vectors is commutative and can be simply resumed to additions of two numbers. The decomposition into pairs of objects is also possible for invertible matrices if they are expressed as transformation matrices from a base i to a base j: $\mathrm{X} = [\mathrm{B}_i \triangleright \mathrm{B}_j]$. Then, the composition XY can be written $\mathrm{X} = [\mathrm{B}_i \triangleright \mathrm{B}_j]$, $\mathrm{Y} = [\mathrm{B}_j \triangleright \mathrm{B}_k]$, and the result is $\mathrm{Z} = \mathrm{XY} = [\mathrm{B}_i \triangleright \mathrm{B}_k]$. In addition, the analytical result of the product of two matrices is also a groupoid composition law as pointed out by Connes (1990):

$$(\mathrm{XY})_{(i,k)} = \sum_j \mathrm{X}_{(i,j)}\mathrm{Y}_{(j,k)}.$$

The decomposition of matrices into pairs of bases explains why the order of the matrices is important when calculating their product (*i.e.* XY is in general different from YX). The groupoid composition law can be imagined spatially as a 'head/tail' condition and also temporally as a 'before/after' condition. It can be used in quantum physics,[6] biology, computer science and for any system that has connections such as graphs and networks (Stewart, 2004).

In these examples, it may be noticed that the groupoid law is based on the existence of two complementary entities: the objects (the points, the bases, the energies[6]) and the operations between these objects (the vectors, the matrices, the frequencies[6]). These operations can be represented by arrows that link the objects.[7] In addition to its composition law, a groupoid must have the following properties: the composition between the arrows is associative and each arrow has an inverse. Groupoids are more general than groups because in the latter the objects and the arrows are two isomorphic entities that cannot be distinguished. Indeed, an element g of a group **G** is also an arrow referenced to the neutral element e because $g.e$ (g is an object transformed by the arrow e) = g (g is an arrow).

A new idea known as 'operator' was also introduced by Cayron (2006). This term has a meaning different from the term 'operation'. An operator is a type of operation and can be expressed by a set of equivalent operations.[8] Moreover, situations or figures that have partial iterative symmetries can often be represented by graphs. Since the vertices and the edges of a graph can be viewed respectively as the objects and the operations of a groupoid, an operator can also be viewed as a type of path in a graph and expressed by a set of equivalent paths. In Appendix *A*, a non-crystallographic example is described in order to familiarize the reader with the idea of operator (as a type of path in a graph or as a type of arrow in a groupoid).

[5] One can understand the simple cosets as types of dangling bonds and double cosets as types of bonds between pairs of atoms.

[6] Connes (1990) makes a clear parallel between the matrix mechanics of Heisenberg in quantum physics and the groupoid composition law of the spectral frequencies of hydrogen given by $\nu_{(E_i,E_j)} + \nu_{(E_j,E_k)} = \nu_{(E_i,E_k)}$, where $\nu_{(E_i,E_j)}$ is the frequency of the spectral line between the energy levels E_i and E_j.

[7] In this paper, we will use equivalently the terms 'operation' and 'arrow'.

[8] For example, a pair of points (P_i, P_j) is an arrow. In the Euclidean space, there is infinity of points (P_i, P_j) similarly placed in their pairs; these pairs form an equivalence class called vector, $\mathbf{V} = \{(P_i, P_j)\}$. A vector is an operator and one can imagine its action on the points by $P_i\mathbf{V} = P_j$.

Table 1
Matrices representing the transformations from a primary cubic crystal into its four Σ3 twinning variants.

They have been chosen in their respective set of type $g_i\mathbf{H}T$ to create a 'harmonious' enumeration of the two-dimensional fractal of Fig. 5(*a*). The geometrical operations corresponding to these matrices are also reported (*m* for a mirror symmetry and *R* for a rotation).

$$T_0 = T = \tfrac{1}{3}\begin{pmatrix} 1 & -2 & -2 \\ -2 & 1 & -2 \\ -2 & -2 & 1 \end{pmatrix} = m_{/(111)}$$

$$T_1 = g_1T = \tfrac{1}{3}\begin{pmatrix} 1 & -2 & -2 \\ 2 & -1 & 2 \\ 2 & 2 & -1 \end{pmatrix} = R([0\bar{1}1], 70.53^\circ) \circ m_{/yx}$$

$$T_2 = g_2T = \tfrac{1}{3}\begin{pmatrix} -1 & 2 & 2 \\ -2 & 1 & -2 \\ 2 & 2 & -1 \end{pmatrix} = R([\bar{1}01], 70.53^\circ) \circ m_{/xz}$$

$$T_3 = g_3T = \tfrac{1}{3}\begin{pmatrix} -1 & 2 & 2 \\ 2 & -1 & 2 \\ -2 & -2 & 1 \end{pmatrix} = R([1\bar{1}0], 70.53^\circ) \circ m_{/xy}$$

4. Geometric and algebraic considerations on multiple twinning

4.1. The groupoid of orientational variants

It has been shown that the orientational variants formed by a structural phase transition $\beta \rightarrow \alpha$ and the operations that link them form a groupoid (Cayron, 2006). Geometrically, the daughter variants were identified to the objects of the groupoid and the misorientations were identified to the arrows between these objects. Algebraically, the details of the structure were obtained by unifying the external symmetries of the parent crystal $\mathbf{G}^\beta$ to the internal symmetries of the daughter crystals $\mathbf{G}^\alpha$ with the help of a transformation matrix T representing the orientation relationship between one daughter crystal and its parent crystal. More precisely, the variants α_i were identified to the simple cosets $g_i^\beta\mathbf{H}$, where $g_i^\beta \in \mathbf{G}^\beta$ and $\mathbf{H}$ is the intersection group between the parent crystal and a daughter crystal (given by $\mathbf{H} = T\mathbf{G}^\alpha T^{-1} \cap \mathbf{G}^\beta$). The types of misorientations between the variants, *i.e.* the operators, were identified to the double cosets $T^{-1}\mathbf{H}g_{ij}^\beta\mathbf{H}T$. The arrow from the variant α_i to α_j and the arrow from the variant α_j to α_k can be composed and the result is the arrow from the variant α_i to the variant α_k, *i.e.* $(\alpha_i \triangleright \alpha_j)\ (\alpha_j \triangleright \alpha_k) = (\alpha_i \triangleright \alpha_k)$. Each operator is written as a set of equivalent arrows $= \{(\alpha_i \triangleright \alpha_j), (\alpha_k \triangleright \alpha_l), \ldots\}$, *i.e.* a set of pairs of variants similarly misoriented. An operator is ambivalent if it transforms the variant α_i into the variant α_j and the variant α_j into the variant α_i. If this is not the case, it is described as polar. To compose the operator O_m^α with the operator O_n^α, $(O_m^\alpha, O_n^\alpha) \rightarrow O_m^\alpha O_n^\alpha$, the groupoid composition rule imposes that the arrival variants of O_m^α must be the starting variants of O_n^α. This composition can be explicitly determined by writing $O_m^\alpha \ni (\alpha_i \triangleright \alpha_j)$, $O_n^\alpha \ni (\alpha_j \triangleright \alpha_k)$ and the resulting operators are those containing the arrows $(\alpha_i \triangleright \alpha_k)$. Since many operators may be obtained, the composition is multivalued. The groupoid composition table characterizes the crystallographic aspect of the transition; some tables were given for the Burgers transition by Cayron (2006) and for the martensitic transitions by Cayron *et al.* (2006).

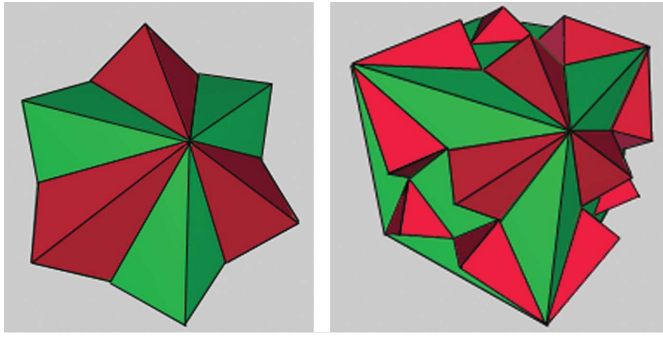

(*a*) (*b*)

Figure 1
Σ3 twin representations: (*a*) a Σ3 twin is in general represented by an association of two crystals of equivalent size, but (*b*) a Σ3 twin results in general from a transformation during mechanical experiments or annealing treatments, and four distinct orientations (four variants) may appear after one twinning transformation (eight are represented but can be associated two by two due to the centrosymmetry of the cubes).

		Σ1	Σ3			
		α^0	α_0^1	α_1^1	α_2^1	α_3^1
Σ1	α^0	Σ1	Σ3	Σ3	Σ3	Σ3
Σ3	α_0^1	Σ3	Σ1	Σ9	Σ9	Σ9
	α_1^1	Σ3	Σ9	Σ1	Σ9	Σ9
	α_2^1	Σ3	Σ9	Σ9	Σ1	Σ9
	α_3^1	Σ3	Σ9	Σ9	Σ9	Σ1

Figure 2
Composition table of the groupoid $\mathbf{\Gamma}^{(0+1)}$ representing an assembly of crystals constituted by a crystal α^0 and its four twinned variants α_0^1, α_1^1, α_2^1 and α_3^1. The operators Σ1 and Σ3 are given with reference to the crystal α^0. The composition of the operators appears as a multivalued function, for example Σ3Σ3 = {Σ1, Σ9}.

4.2. The groupoids of simple twinning

Simple Σ3 twinning in face-centred cubic (f.c.c.) materials may be imagined as a phase transition with $\mathbf{G}^\alpha = \mathbf{G}^\beta = \mathbf{G}$ and $T = T^{-1}$ the matrix representing the mirror symmetry through the (111) plane (see Table 1). The intersection group

$$\mathbf{H} = \mathbf{G} \cap T\mathbf{G}T \tag{6}$$

contains 12 symmetry operations and in consequence the number of variants is $N^\alpha = |\mathbf{G}|/|\mathbf{H}| = 4$. Let us call α^0 the primary crystal (parent crystal), and α_0^1, α_1^1, α_2^1 and α_3^1 the four twins of this crystal (daughter crystals). More generally, the *i*th twin of the *n*th generation will be denoted α_i^n.The five crystals are represented in Fig. 1(*b*) (this figure is probably closer to the actual algebraic developments of twinning and coset partitioning than the classical representation of Fig. 1*a*). The four variants α_0^1, α_1^1, α_2^1 and α_3^1 are linked to the primary crystal α^0 by a Σ3 operator, between them by a Σ9 operator and to themselves by a Σ1 operator: $(\alpha_0 \triangleright \alpha_i^1) \in \Sigma3$, $(\alpha_i^1 \triangleright \alpha_j^1) \in \Sigma9$ for $i \neq j$ and $(\alpha_i^1 \triangleright \alpha_i^1) \in \Sigma1$. Three groupoids may be defined:

(i) $\mathbf{\Gamma}^{(0)}$ is constituted by one object (α^0) and one arrow ($\alpha^0 \triangleright \alpha^0$) forming one operator ($\Sigma 1 = \mathbf{G}$).

(ii) $\mathbf{\Gamma}^{(1)}$ is constituted by four objects (α_0^1, α_1^1, α_2^1 and α_3^1), 16 arrows ($\alpha_i^1 \triangleright \alpha_j^1$) with $(i, j) \in [0, 3]^2$ partitioned into two operators ($\Sigma 1$ and $\Sigma 9$). This is a groupoid of orientational variants described in §4.1. The four variants are algebraically identified with the four cosets $g_i\mathbf{H}$ that constitute the set $\mathbf{G}/\mathbf{H}$ and the two operators expressed in a basis of α^0 are the double cosets of the set $\mathbf{G}\backslash\mathbf{H}/\mathbf{G}$: $\Sigma 1 = \mathbf{H}$ and $\Sigma 9 = \mathbf{H}g_1'\mathbf{H}$.

(iii) $\mathbf{\Gamma}^{(0+1)} = \mathbf{\Gamma}^{(0)} \cup \mathbf{\Gamma}^{(1)}$, which is a union of groupoids is constituted by 5 objects, 25 arrows partitioned into 3 operators ($\Sigma 1$, $\Sigma 3$ and $\Sigma 9$). Its composition table is reported in Fig. 2. It may be checked in this table that the composition of two $\Sigma 3$ can be either a $\Sigma 1$ or a $\Sigma 9$ operator. One may add that the result is $\Sigma 1$ with a probability of 1/4 and is $\Sigma 9$ with a probability of 3/4. Only arguments based on calculations of energies can modify significantly these crystallographic probabilities (but in this study, we will only consider crystallographic arguments).

4.3. The groupoids of multiple twinning

By considering simple twinning as a phase transition with $\beta = \alpha$, multiple twinning $\Sigma 3^n$ may now be imagined as a series of phase transitions $\beta \rightarrow \alpha \rightarrow \beta \rightarrow \alpha \rightarrow \beta$ *etc.* In Cayron (2006), we raised the following questions: is there a general formula to calculate the number of variants and the number of operators of the nth generation? Do these numbers increase to infinity with n? We do not know the general solution to these questions but we will answer them in the special case of multiple twinning.

The approach of the previous section can be generalized, the variants of generation n and the operations that link them form a groupoid $\mathbf{\Gamma}^{(n)}$. This groupoid can be associated with the groupoids of the previous generations $\mathbf{\Gamma}^{(i)}$ with $i < n$ to form a groupoid denoted $\mathbf{\Gamma}^{(0+1+\ldots+n)}$. This last groupoid and its subgroupoids form a structure similar to a Russian doll. Its algebraic details remain to be fully determined; such a study implies the generalization of the use of cosets and double cosets to multiple cosets linked by a transformation matrix.[9] However, we will see in the following that some basic geometrical considerations are actually sufficient to determine the operators and their composition table.

4.4. Three-dimensional fractal representations

We may imagine all the twinning variants in three dimensions: (i) by representing the primary crystal with a tetrahedron constituted by its four {111} planes, (ii) by creating its four variants by applying the {111} mirror symmetries, and (iii) by repeating this process. The topology makes this approach impossible for orders higher than three (it is the well known problem of tetrahedra packing). However, all the variants can be created if one decreases the size of the tetrahedra by a factor of two at each generation of the process. The result is the three-dimensional fractal illustrated in Fig. 3. This fractal is a more complex version than the three-dimensional Kepler fractal in which the tetrahedra are only translated but not rotated. The representation of Fig. 3 is a convenient way to illustrate the orientations of all the multiply twinned crystals on the same drawing. It is particularly illustrative for twinning in $\bar{4}3m$ crystals (such as sphalerite). It may be noticed that, owing to the absence of centrosymmetricity, the [111] and $[\bar{1}\bar{1}\bar{1}]$ directions are not equivalent (compare Figs. 3*a* and *b*). For $m3m$ crystals, such as f.c.c. metals, the tetrahedra can be substituted by cubes; the generated fractal is then illustrated in Fig. 4. This fractal is constituted by interpenetrated cubes, the twinned cubes of the $(n + 1)$th generation are positioned at the corners of the nth-generation cubes. By construction, the whole fractal has the same symmetries as for the primary

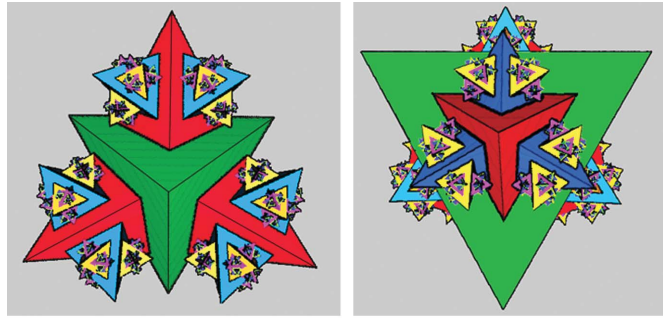

(*a*) (*b*)

Figure 3
Three-dimensional tetrahedral fractal representation of multiply twinned crystals ($\bar{4}3m$) inherited from the same primary crystal α^0 (in green), viewed (*a*) in the [111] direction and (*b*) in the $[\bar{1}\bar{1}\bar{1}]$ direction of α^0 (the two directions are not equivalent because a tetrahedron is not centrosymmetric). This fractal is built from twinned tetrahedra reduced in size by a factor of two at each generation and lying in the centres of the faces of the tetrahedra of the preceding generation. Distinct colours are associated with the orders n of the fractal.

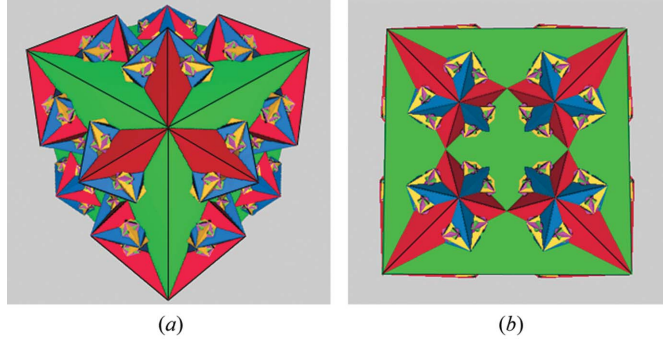

(*a*) (*b*)

Figure 4
Three-dimensional cubic fractal representation of multiply twinned crystals ($m3m$) viewed (*a*) in the [111] direction and (*b*) in the [100] direction of α^0. This fractal has been built with the same misorientations and displacements as those of Fig. 3 (the tetrahedra have only been substituted by cubes).

[9] The orientations of four crystals of first generation are given in reference to the orientation of the primary crystal α^0: the orientation of α_0^1 is given by $\mathbf{H}T$, the orientation of α_1^1 by $g_1\mathbf{H}T$, α_2^1 by $g_2\mathbf{H}T$ and α_3^1 by $g_3\mathbf{H}T$. Each α_i^1 becomes the parent crystal of the variants of second generation α_j^2. The orientations of these variants in reference to the primary crystal α^0 are given by the set of matrices $g_i\mathbf{H}Tg_j\mathbf{H}T$. More generally, the orientations of the twinned crystals at any order n are given by the sets of type $g_i\mathbf{H}Tg_j\mathbf{H}Tg_k\mathbf{H}T\ldots$ (n times) with $(i, j, k, \ldots) \in [0, 3]^n$.

crystal. For example, it may be checked that the cubic fractal viewed in ⟨111⟩ and ⟨100⟩ directions (Figs. 4*a* and *b*) exhibits the two-dimensional 3*m* and 4*mm* symmetries, respectively.

From these figures, it appears that the number of distinct variants at the *n*th generation is given by = 4.3^n, for $n \geq 1$ (see also Wilbrandt, 1980; Gottstein, 1984). We have seen that the assembly of grains twinned to the *n*th generation constitutes the groupoid $\mathbf{\Gamma}^{(0+1+\ldots+n)}$ and can be represented by a fractal (stopped at the *n*th generation). Such assembly has its own CSL, which will be denoted CSL^n. It is the intersection of the lattices of all these crystals. Therefore, the CSL^n has the same symmetry elements as for the primary crystal and it can be referenced in the primary crystal basis with a matrix of type aE, where E is the 3×3 identity matrix and $a \in \mathbb{N}$. Moreover, the CSL^n can also be expressed with integer coordinates in the reference bases of all the twinned crystals, which means that the CSL^n matrix multiplied by any transformation matrix given in equation (1) with $\Sigma = 3^n$ should be equal to an integer matrix. Since the a_{ij} coefficients in equation (1) are co-prime (they have no common divisor except 1), such a condition leads to

$$\mathrm{CSL}^n = \begin{bmatrix} 3^n & 0 & 0 \\ 0 & 3^n & 0 \\ 0 & 0 & 3^n \end{bmatrix}. \qquad (7)$$

It follows that the volume of the CSL^n lattice is $\Sigma^{\mathrm{multi}} = 3^{3n}$. This result could also probably be derived from the general formula suggested by Gertsman (2001*b*).

4.5. Macro/microscopic examples of three-dimensional fractal shapes

We recall that the fractal representation is just a convenient way that will help us to visualize the symmetries and to simplify the calculations. However, we may wonder if such shapes can exist in nature. Indeed, with perfect isotropic growth conditions, the macroscopic shape of an assembly of multiply twinned crystals could be close to Fig. 3 for $\bar{4}3m$ structures or to Fig. 4 for *m*3*m* structures. Even if isotropic conditions are rarely found in mineralogy, multiple twins of diamond and sphalerite crystals can sometimes look like Fig. 3(*b*) – the reader is invited to look at the photographs reported by Palache (1932). The star polyhedral gold nanoparticles recently discovered by Burt *et al.* (2005) also exhibit shapes close to Fig. 3 (with $n = 2$). Another case is probably the fractal structure of a dislocation-free bicrystal silicon ribbon studied by Cheng (1994). He reported angles of reentrant corners (141 and 109.5°) that correspond respectively to some rotation angles of the Σ9 operator ($180 - 141 \simeq 38.94°$) and of the Σ3 operator ($180 - 109.5 = 70.5°$ = angle between two {111} planes). An EBSD study of this ribbon could be interesting to confirm that the orientations of the crystals are of type $\Sigma 3^n$. Fractal structures are also obtained by phase transformations very similar to the twinning transformation. The hyperbranched structures of CdTe or CdSe nanocrystals are constituted of branched tetrapods (Milliron *et al.*, 2004) resulting from the alternating transitions between the cubic sphalerite phase and the hexagonal wurtzite phase: sphalerite transforms into four wurtzite branches in the ⟨111⟩ directions (as in the twinning case), and each wurtzite branch transforms into two sphalerite branches in the two +**c** and −**c** directions.

5. The $\Sigma 3^\xi$ semigroup of multiple twinning

The whole three-dimensional fractal represents the whole twinning groupoid $\mathbf{\Gamma}^\infty = \mathbf{\Gamma}^{(0+1+\ldots+n)}$ with $n = \infty$. What is the relation between the free group $\Sigma 3^\omega$ introduced by Reed *et al.* (2004) and $\mathbf{\Gamma}^\infty$? In the group $\Sigma 3^\omega$, the four strings that begin with the letters *a*, *b*, *c* and *d* correspond to the four branches of the fractal. Each string of the free group $\Sigma 3^\omega$ encodes a path on the fractal. It must be remembered that the four letters represent 180° rotation matrices that were chosen in the sets $\mathbf{H}T$, $g_1\mathbf{H}T$, $g_2\mathbf{H}T$ and $g_3\mathbf{H}T$. The relative simplicity of the $\Sigma 3^\omega$ structure results from this 'not so arbitrary' choice. Other choices of representatives in those sets lead to different algebraic structures that are all substructures of $\mathbf{\Gamma}^\infty$. In order to convince the reader, we are creating a structure denoted $\Sigma 3^\xi$, which will be proved to be *not isomorphic* to $\Sigma 3^\omega$, but that can also be used to encode the $\Sigma 3^n$ operators. The representatives are chosen in the sets $\mathbf{H}T$, $g_1\mathbf{H}T$, $g_2\mathbf{H}T$ and $g_3\mathbf{H}T$ such that the faces of the tetrahedra in the developed representation of the fractal of Fig. 3 (Fig. 5*a*) are 'harmoniously' enumerated. These matrices T_0, T_1, T_2, T_3 and their corresponding geometrical meaning are reported in Table 1.

5.1. Calculation of the operators

The whole fractal and the associated $\Sigma 3^n$ operators can be constructed from the four T_i matrices of Table 1 by calculating the matrix products $T_iT_jT_k \ldots T_l$. In all the following, these products will be written as strings

$$T_iT_jT_k \ldots T_l = ijk \ldots l. \qquad (8)$$

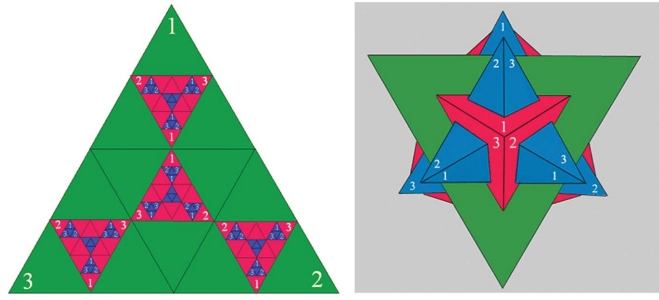

(*a*) (*b*)

Figure 5
Enumeration of the faces of the tetrahedra. (*a*) Developed representation of the fractal of Fig. 3 (in fact, to avoid overlapping of the faces, the scaling factor is not 1/2 as for the three-dimensional fractal but 1/4). This two-dimensional fractal is usually called a Sierpinsky fractal. The faces have been enumerated in such a way that the arrangement of the numbers in this figure respects a simple 'harmonious' rule. (*b*) The corresponding numbers are reproduced in the three-dimensional fractal limited to $n = 2$.

Table 2
$\Sigma 3^n$ operators (reproduced here up to $n = 6$).

For space reasons, the CSL rotation matrices are given only up to $n = 4$ with only the integer coefficients a_{ij} of expression (1). For $n > 4$, for more visibility, ny should be read $\Sigma 3^n y$ (for example $5a$ is $\Sigma 3^5 a$). The polar operators are marked by +/− signs, the others are ambivalent operators. The string coding $i\,j\,\ldots\,l$ corresponds to the matrix product given by the formula (8) with the matrices of Table 1.

Order 1

Σ1
[1 −2 −2]
[2 −1 2]
[2 2 −1]
1
60.000 [1, 1, 1]

Order 2

Σ9
[−7 −4 −4]
[4 1 −8]
[4 −8 1]
1 1
38.942 [0, −1, 1]

Order 3

Σ27a
[−23 10 10]
[−10 −25 2]
[−10 2 −25]
1 1 1
31.586 [0, 1, −1]

Σ27b
[7 −26 −2]
[−22 −7 14]
[14 2 23]
1 1 2
35.431 [0, 2, 1]

Order 4

Σ81+a
[23 −16 −76]
[64 −41 28]
[−44 −68 1]
1 1 1 2
38.376 [−1, −3, −5]

Σ81−a
[41 −16 68]
[64 −23 −44]
[28 76 1]
1 1 2 2
38.376 [1, 5, −3]

Σ81b
[−49 8 −64]
[−8 79 16]
[64 16 −47]
1 1 2 1
38.942 [1, 4, 1]

Σ81c
[−55 44 −40]
[−20 −65 −44]
[−56 −20 55]
1 1 2 3
54.532 [2, −3, −2]

Σ81d
[17 56 56]
[−56 49 −32]
[−56 −32 49]
1 1 1 1
60.408 [−4, 3, 4]

Order 5

5a
1 1 1 1 1
7.356 [0, −1, 1]

5b
1 1 2 3 1
12.213 [1, −3, −1]

5c
1 1 2 2 3
31.586 [1, 4, 1]

5+d
1 1 1 2 3
35.431 [−2, 4, −5]

5−d
1 1 2 3 3
35.431 [5, 2, −4]

5+e
1 1 1 2 1
43.076 [−1, −3, −11]

5−e
1 1 2 1 1
43.076 [3, −11, −1]

5+f
1 1 1 1 2
43.076 [−9, 7, −1]

5−f
1 1 2 2 2
43.076 [1, −7, −9]

5g
1 1 2 1 2
43.076 [5, 9, −5]

5+h
1 1 2 1 3
49.753 [6, 7, −1]

5−h
1 1 2 3 2
49.753 [−7, 6, 1]

5i
1 1 2 2 1
49.753 [5, −6, −5]

5j
1 1 1 2 2
60.0 [−11, 1, −11]

Order 6

6+a
1 1 1 2 2 1
11.247 [−3, 1, 2]

6−a
1 1 2 2 1 1
11.247 [−1, −3, −2]

6+b
1 1 2 1 2 3
22.087 [5, 9, 1]

6−b
1 1 2 3 2 3
22.087 [9, −5, −1]

6c
1 1 2 1 3 1
22.087 [7, −7, −3]

6d
1 1 2 2 2 3
28.608 [0, 5, −8]

6e
1 1 2 3 2 1
28.608 [9, 2, −2]

6+f
1 1 1 1 2 3
28.608 [7, −6, 2]

6−f
1 1 2 3 3 3
28.608 [6, 2, 7]

6+g
1 1 1 2 3 2
28.608 [−3, −4, −8]

6−g
1 1 2 1 3 3
28.608 [8, 4, −3]

6h
1 1 2 2 2 1
31.285 [0, −2, −7]

6+i
1 1 1 1 2 2
31.285 [−4, −6, 1]

6−i
1 1 1 2 2 2
31.285 [−6, 4, −1]

6+j
1 1 1 1 2 1
38.376 [17, 5, −1]

6−j
1 1 2 1 1 1
38.376 [1, −17, −5]

6+k
1 1 2 2 1 3
38.376 [11, 5, −13]

6−k
1 1 2 3 3 2
38.376 [−11, −5, 13]

6+l
1 1 1 2 1 3
38.942 [−5, 4, −11]

6−l
1 1 2 3 2 2
38.942 [−5, −11, 4]

6m
1 1 2 1 2 1
38.942 [8, −7, −7]

6n
1 1 1 2 1 1
44.383 [−1, 0, −5]

6+o
1 1 2 2 1 2
44.383 [−4, 3, 1]

6−o
1 1 2 1 1 2
44.383 [3, 4, −1]

6p
1 1 1 2 3 3
47.126 [0, 13, 8]

6+q
1 1 2 2 3 1
47.126 [6, −14, −1]

6−q
1 1 2 3 3 1
47.126 [−14, −1, −6]

6+r
1 1 2 2 3 2
47.126 [5, 12, −8]

6−r
1 1 2 1 1 3
47.126 [8, 12, −5]

6+s
1 1 1 2 2 3
49.701 [15, −1, −17]

6−s
1 1 2 2 3 3
49.701 [15, 17, 1]

6+t
1 1 1 2 3 1
49.701 [−15, 11, 13]

6−t
1 1 2 3 1 1
49.701 [−11, −15, −13]

6+u
1 1 1 2 1 2
54.145 [−5, 9, 14]

6−u
1 1 2 1 2 2
54.145 [−5, −9, 14]

6+v
1 1 1 1 1 2
54.145 [9, 11, 10]

6−v
1 1 2 2 2 2
54.145 [−9, 11, 10]

6w
1 1 2 3 1 2
54.532 [8, 8, 5]

6+x
1 1 2 1 3 2
58.997 [−11, −19, 15]

6−x
1 1 2 3 1 3
58.997 [−11, −19, −15]

6y
1 1 1 1 1 1
60.408 [10, 10, 13]

The operations are encoded by the strings and the operators are encoded by sets of equivalent strings. The calculations can be reduced to the minimum if the symmetries of the fractal (*i.e.* the symmetries of the primary crystal) are taken into consideration. Indeed, the fractal is constituted by four main branches on the four threefold axes of α^0, which are obtained by taking as the first matrix in the product (8) T_0 for branch 0, T_1 for branch 1, T_2 for branch 2, and T_3 for branch 3. Since these branches are all geometrically equivalent, all the operations can be done with only one branch. We choose branch 1, *i.e.* the one starting with T_1. These geometrical considerations explain why there is only one $\Sigma 3$ operator. The first variant on this branch is α_1^1. From this variant, three new variants α_1^2, α_2^2 and α_3^2 can be created, and they are all equivalent due to the threefold symmetry of this branch. Therefore, to calculate the other operators, we can limit ourselves to calculate the matrix products that start with T_1T_1, *i.e.* the strings 11 ... These geometrical considerations explain why there is only one $\Sigma 9$ operator. From α_1^2, three new variants can be created, but two are equivalent due to the mirror symmetry on the plane (011). Therefore, there are only two $\Sigma 27$ operators: one containing the string 111 (= Σ27a) and another one containing to the string 112 (= Σ27b). From this step ($n = 3$), each variant of generation n will generate three new variants of generation $n + 1$, with the exception of the one that keeps the (011) plane of α^0 as a mirror plane. Consequently, for the orders $n > 3$, all the operators can be recursively generated with the help of five distinct types of operations ($\alpha_i^n \triangleright \alpha_j^{n+1}$).

(*a*) If α_i^n keeps having a mirror symmetry through the initial mirror plane (011), the operation ($\alpha_0 \triangleright \alpha_i^n$) is of type T_1^n = 111 ... 1 (n terms). Three new variants and two new operators can be created from α_i^n: the first operator contains the string 111 ... 11 ($n + 1$ terms) = $T_1^nT_1$, and the second one contains the string 111 ... 12 ($n + 1$ terms) = $T_1^nT_2$. Both are illustrated in Fig. 6 (in the case of $n = 4$).

(*b*) If α_i^n is not symmetric through the initial mirror plane (011), the operation ($\alpha_0 \triangleright \alpha_i^n$) is of type M = 11 ... 2 ... i (n terms). Three new variants and three new operators can be created from α_i^n: they contain the strings 11 ... 2 ... ij ($n + 1$ terms) = MT_j, $j \in \{1, 2, 3\}$. If $j = i$, the connection is a 'forward' connection; if $j \neq i$, the first index h before i with $h \neq i$ must be determined and if $j = h$ the connection is a 'circular' one, and if $j \neq h$ the connection is a 'zigzag' one.

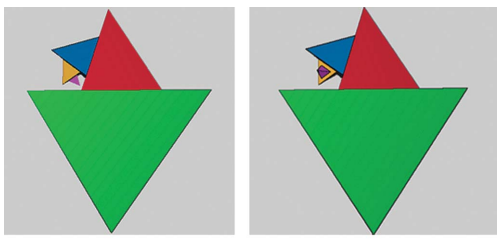

(*a*) (*b*)

Figure 6
Three-dimensional graphical representation of two $\Sigma 81$ operators: (*a*) Σ81d containing the string 1111, (*b*) Σ81+a containing 1112.

These symmetry considerations allow the creation of the minimum number of variants required to compute the construction of the fractal, all the other variants are deduced by the symmetries of the primary crystal α^0 (*i.e.* the point group **G**). At the nth generation, the number of distinct operators is easily deduced from this geometrical approach. Indeed, it respects the arithmetic geometric sequence $N_{n+1}^{\rm op} = 3N_n^{\rm op} - 1$ with $N_2^{\rm op} = 1$. In consequence,

$$N_n^{\rm op} = \tfrac{1}{2}(3^{n-2} + 1), \quad \text{for } n \geq 2. \tag{9}$$

By construction, $\Sigma 3^\xi$, the set of strings based on the four indices (0, 1, 2, 3) is a semigroup.[10] $\Sigma 3^\xi$ is not a group because the indices 1, 2 and 3 have no inverse. Of course, $\Sigma 3^\xi$ is not isomorphic to $\Sigma 3^\omega$.

5.2. Names of the operators

Once the matrices M representing the operators $\Sigma 3^n$ are determined (with their string code), the operators can be named according to the following method: (*a*) calculate for each matrix M the set **G***M***G** of polarly cubically equivalent matrices (see footnote 3), (*b*) choose in this set the rotation with the minimum angle as representative and (*c*) order the operators according to these minimum angles. For example, the rotations with minimum angles of 31.58 and 35.43° are associated with the operators Σ27a and Σ27b, respectively. This way of ordering is equivalent to comparing the norms of the quaternions. However, as already noticed by Reed *et al.* (2004), many distinct operators can have the same representative minimum angle. A solution was proposed by these authors for quaternions, however, here, since only the matrix expressions are used, we have decided to choose another ordering rule. For each rotation matrix representative of the operator (*i.e.* with the minimum angle), we also consider the orientation of its rotation axis, a second ordering is then realized (if necessary) by calculating the minimum scalar product between this axis and the ⟨111⟩ axes. Since this ordering sometimes is not enough because two distinct operators can have the same minimum rotation angle and the same angle between the rotation axis and the ⟨111⟩ axes, a third ordering rule is sometimes required by calculating the minimum scalar product between the rotation axis and the ⟨100⟩ axes. Once the operators have been ordered, they are identified with letters. Since the alphabet is not large enough for twinning orders $n > 6$, it has been extended according to the rule: $a, \ldots, z, aa, ab, \ldots, az, ba, bb, \ldots, bz, \ldots$ *etc.* The naming and ordering of the operators takes most of the computing time (one minute for order $n = 8$) because it implies matrix calculations. The ordered operators are reported in Table 2 for twinning order $n \leq 6$ (the list for higher twinning order is available on demand). It may be noted that the lists given in some previous studies (Gottstein, 1984; Andreeva & Firsova, 1996) are not quite complete. We also would like to stress that it is possible to distinguish the complementary polar

[10] A semigroup is an algebraic structure consisting of a set closed under the associative binary operation. A group is a semigroup in which there is a neutral element and all the elements have an inverse.

operators (see footnote 3). For example, the two Σ81a operators with a minimum angle of 38.376° and rotation axes of type ⟨135⟩ were distinguished; we called them $\Sigma3^4$+a and $\Sigma3^4$−a. Indeed, if we denote T^4_{+a} = 1112 the matrix associated with $\Sigma3^4$+a and T^4_{-a} = 1122 the matrix associated with $\Sigma3^4$−a (given in Table 2), the reader may check (by computing) that the associated set of polarly cubically equivalent matrices forming the $\Sigma3^4$+a and $\Sigma3^4$−a operators, *i.e.* $\mathbf{G}T^4_a\mathbf{G}$ and $\mathbf{G}T^4_{-a}\mathbf{G}$, with $\mathbf{G}$ the $m3m$ point group, do not intersect: $T^4_{-a} \notin \{g_i T^4_{+a} g_j, (g_i, g_j) \in \mathbf{G}^2\}$ but $T^4_{-a} \in \{g_i T^4_{+a}{}^{-1} g_j, (g_i, g_j) \in \mathbf{G}^2\}$. The operator $\Sigma3^4$+a and $\Sigma3^4$−a are complementary polar operators.

5.3. Two-dimensional graph and pole-figure representations

The different operators corresponding to the $\Sigma3^\xi$ semigroup can be represented on a graph similar to the one introduced by Reed *et al.* (2004) (the only slight difference is the distinction we have made in the labelling between the polar and ambivalent operators). This graph can be redrawn to obtain a two-dimensional fractal graph based on Templar-style crosses, as shown in Fig. 7 (limited here to $n \leq 5$ for space reasons). In this figure, the operators are the centres of the crosses and the variants are the tips. This graph is called a Cayley graph (used by mathematicians to encode the free group based on two generators). One may observe that the types of connections between the operations such as the circular or zigzag connections also appear in this two-dimensional fractal scheme.

The twinned variants can also be represented by drawing their orientations on a pole figure in one of the reference bases of the primary crystal, as illustrated for twinning orders $n \leq 5$ in Fig. 8 (for higher orders there are too many points and only the densities could be represented). Such figures were already presented by Gottstein (1984) but were incomplete because of some missing operators. As already calculated by Wilbrandt (1980), it is very difficult to distinguish a random misorientation from a $\Sigma3^n$ operator for twinning orders n higher than 5. Some special patterns can also be noticed in these pole figures (such as the circles). These come from operators that have very close minimum rotation angles (such as the Σ81+a, Σ81−a and Σ81b operators). As the order n increases, the number of operators with close or even exact minimum rotation angles increases and the number of singular patterns increases (as confirmed by simulations of pole figures of operators with equal rotation angles and random rotation axes, not presented here).

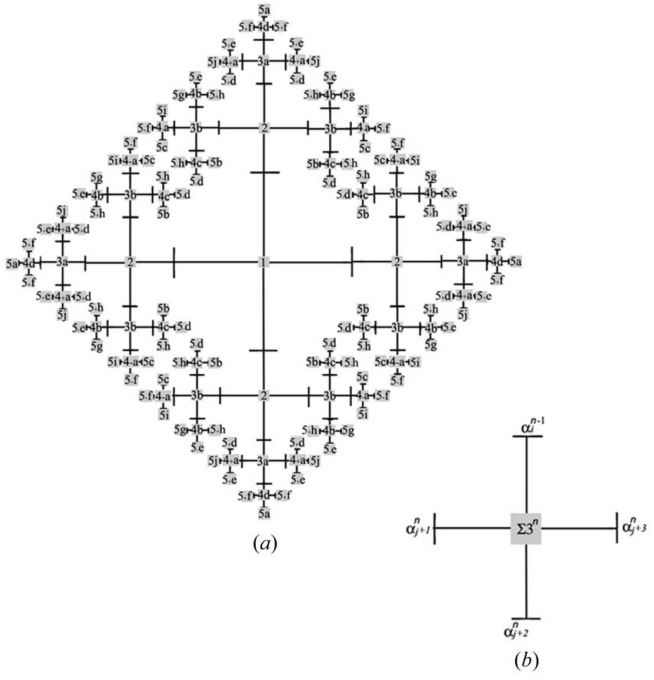

Figure 7
(*a*) Two-dimensional fractal graph of the multiply twinned variants and $\Sigma3^n$ operators (up to order $n = 5$). The fractal is built from a Templar-style cross represented in (*b*) reduced in size by a factor of two at each generation step; the crosses are joined at the tips of those of the preceding generation. The variants are the tips of the crosses (not labelled) and the $\Sigma3^n$ operators are the centres of the crosses. This two-dimensional graph is usually called a Cayley graph.

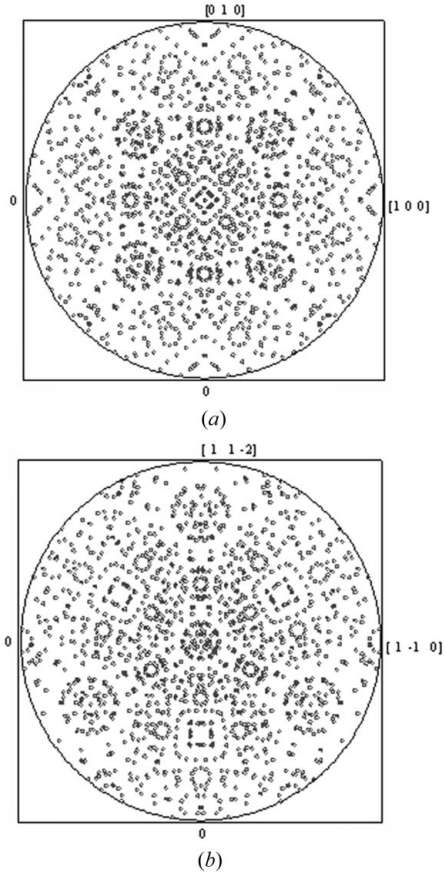

Figure 8
Pole figures of an assembly of multiply twinned crystals linked to the primary crystal α^0 by $\Sigma3^n$ operators with $n \leq 5$; the ⟨111⟩ directions are represented (*a*) in the [001] direction and (*b*) in the [111] direction of α^0.

5.4. Comparison of the $\Sigma 3^{\xi}$ semigroup with the $\Sigma 3^{\omega}$ group

The $\Sigma 3^{\xi}$ semigroup (based on the indices 0, 1, 2, 3) and the $\Sigma 3^{\omega}$ free group (based on the letters a, b, c, d) are represented by the same graph although these two structures are not isomorphic.

In the $\Sigma 3^{\omega}$ group, all of the letters play the same role in the strings, and they can be interchanged. Moreover, the simplification rule $aa = bb = cc = dd = \emptyset$ with $\emptyset$ the empty string (coding the identity matrix) is based on the choice of 180° rotation matrices in the four sets $g_i\mathbf{H}T$ that define the orientations of the variants with $i \in [0, 3]$. This rule makes the string representation unique and consequently makes $\Sigma 3^{\omega}$ free.

In the $\Sigma 3^{\xi}$ semigroup, only the indices 1, 2 and 3 are equivalent. The index 0 appears only one time in the whole $\Sigma 3^{\xi}$ graph (it begins the strings that codes the branch 0). In fact, the index 0 (and the associated matrix T_0) is 'special' and cannot be treated as the three other indices. Since 0 represents a mirror symmetry, it obeys the simplification rule $00 = \emptyset$. Consequently, $000\ldots$ (n times) is equal to 0 if n is odd, and to $\emptyset$ if n is even, whereas the strings $111\ldots, 222\ldots$ or $333\ldots$ (n times) cannot be reduced. The asymmetry between the index 0 and the three others has a temporal meaning if twinning is considered as a temporal process. Let us imagine a progressive twinning by annealing and recrystallization from a variant of order n, the indices 1, 2 and 3 produce three new crystals of order $n + 1$, whereas the index 0 corresponds to a crystal of generation $n - 1$ that was already produced in the past. The composition with the index 0 means that there is a unique way to go back to the past, and the composition with the indices 1, 2, 3 means that there are three equivalent (locally symmetric) ways to go to the future. There is no simplification rule between the indices (1, 2, 3). The simplification is realized only between the index 0 and the three indices (1, 2, 3). What is the rule? For example, how could we simplify the string that corresponds to 112.012 = 112012? More generally, how could we simplify the string $h\ldots i.0j\ldots k = h\ldots i0j\ldots k$? The specific matrices T_i for $i \in [1, 3]$ that we have chosen in the sets $g_i\mathbf{H}T$ to harmoniously enumerate the faces of the tetrahedra on the two-dimensional developed fractal (see §4.4) give the following rule:

$$\ldots \mathrm{a}i0j\mathrm{b}\ldots = \ldots \mathrm{a}k\mathrm{b}\ldots \qquad (10)$$

with
$$\begin{cases} \text{if } i = j,\ k = 0 \\ \text{if } i \neq j,\ k \text{ is the unique element } \in \{1, 2, 3\}\backslash\{i, j\} \end{cases}$$

This property comes from the fact that 101 = 0, 102 = 3, 103 = 2, which can be checked by calculating the matrix products (8) with the matrices given in Table 1 (the other combinations are true due to the equivalence of the 1, 2, 3 indices).

6. Composition of the $\Sigma 3^{n}$ operators

The idea of CSL was initially introduced to characterize the grain boundaries between two crystals. When metallurgists became interested in triple junctions, a method to compose the CSL rotations and to determine the CSL of an assembly of grains was developed. Most of the studies were restricted to finding a rule for the composition of the Σ numbers that appear in expression (1), and few studies treated the composition of the operators.

6.1. Composition of the Σ numbers[11]

It was believed for a long time that the Σ numbers in the CSL matrix expressions (1) are numbers that can be multiplied without precaution. It was believed for example that the three Σ numbers which determine the respective misorientations between three crystals (indexed by 1, 2, 3) follow the rule $\Sigma_{13} = \Sigma_{12}\Sigma_{23}$, where Σ_{ij} is the Σ value of the misorientation matrix between the crystal i and the crystal j. This rule was puzzling because it does not respect the symmetry of the problem, *i.e.* the three crystals do not play similar roles. Actually, it was proved to be wrong. The correct Σ composition rule was proposed by Miyazawa *et al.* (1996), with a demonstration given by Gertsman (2001*a*). It is derived from the following relationship:

$$\Sigma_{13} = \Sigma_{12}\Sigma_{23}/\beta_{123}^2, \qquad (11)$$

where β_{123} is the greatest common odd divisor of the quaternion produced by the multiplication of the two quaternions describing the two generating CSL misorientations.[12] This property is general; therefore, we also have

$$\Sigma_{12} = \Sigma_{13}\Sigma_{32}/\beta_{132}^2, \qquad (12)$$

$$\Sigma_{23} = \Sigma_{21}\Sigma_{13}/\beta_{213}^2. \qquad (13)$$

By multiplying equations (11) and (12), and simplifying the result by using the equality $\Sigma_{23} = \Sigma_{32}$ (because the inverse of the matrix in equation (1) is its transpose), it follows that $\Sigma_{23} = \Sigma_{32} = \beta_{123}\,\beta_{132}$. Similarly, by using equations (12) and (13), it follows that $\Sigma_{13} = \Sigma_{31} = \beta_{132}\,\beta_{213}$ and, by using equations (11) and (13), it follows that $\Sigma_{21} = \Sigma_{12} = \beta_{123}\beta_{213}$. By writing $\beta_{213} = p_1$, $\beta_{123} = p_2$ and $\beta_{132} = p_3$, *i.e.* $\beta_{ijk} = p_j$, the three equalities can be summarized by using a simple rule:

$$\Sigma_{ij} = \Sigma_{ji} = p_i p_j \quad \text{for } (i, j) \in \{1, 2, 3\}. \qquad (14)$$

This formula has been shown by Miyazawa *et al.* (1996) and Gertsman (2001*a*), but we have preferred to show a complete demonstration.[12] This rule is illustrated for three crystals in Fig. 9. This approach can also be generalized to four crystals.[13] The rule (14) indicates that two Σ numbers ΣX and ΣY can be composed if and only if they have a common integer p_j in their decomposition, *i.e.* $\Sigma\mathrm{X} = p_i p_j$ and $\Sigma\mathrm{Y} = p_j p_k$ and that the result of this composition is $\Sigma\mathrm{Z} = p_i p_k$. By denoting $\Sigma\mathrm{X} = \Sigma_{(p_i p_j)}$, $\Sigma\mathrm{Y} = \Sigma_{(p_j p_k)}$ and $\Sigma\mathrm{Z} = \Sigma_{(p_i p_k)}$, one can write the composition rule in the form

[11] This is a general theoretical approach; the application to the particular case of $\Sigma 3^{n}$ CSL numbers is given at the end of the section.

[12] β_{123} was denoted simply β by Gertsman (2001*a*), but this notation is not accurate because it is assumed that this number is the same for all the Σ combinations, whereas in general $\beta_{123} \neq \beta_{132} \neq \beta_{213}$.

[13] For four crystals, one can write $\Sigma_{ij} = \Sigma_{ji} = p_i p_j$ for $(i, j) \in \{1, 2, 3\}^2$, $\Sigma_{ij} = \Sigma_{ji} = q_i q_j$ for $(i, j) \in \{1, 2, 4\}^2$, $\Sigma_{ij} = \Sigma_{ji} = r_i r_j$ for $(i, j) \in \{1, 3, 4\}^2$ and $\Sigma_{ij} = \Sigma_{ji} = s_i s_j$ for $(i, j) \in \{2, 3, 4\}^2$, which could be illustrated on a tetrahedron with schemes similar to that of Fig. 9 for its four faces.

Table 3
Composition table of the $\Sigma 3^n$ operators for $n \leq 4$.

The composition is given for the column m and the line n by $\Sigma 3^m\ \Sigma 3^n = \{\Sigma 3^q\}$. It is a multivalued composition. For space reasons, the resulting operators $\Sigma 3^q z$ are denoted by qz (for example 5a is $\Sigma 3^5$a).

$m \setminus n$	Σ3	Σ9	Σ27a	Σ27b	Σ81+a	Σ81−a	Σ81b	Σ81c	Σ81d
Σ3	0 2	1 3a 3b	2 4−a 4d	2 4+a 4b 4c	3b 5c 5+f 5i	3a 5−d 5−e 5j	3b 5+e 5g 5−h	3b 5b 5+d 5+h	3a 5a 5−f
Σ9	1 3a 3b	0 2 4−a 4+a 4b 4c 4d	1 3b 5a 5−d 5−e 5−f 5j	1 3a 3b 5b 5c 5+d 5+e 5+f 5g 5+h 5−h 5i	2 4b 4c 6+a 6d 6h 6−k 6−o 6−q 6−r 6+s 6+v	2 4−a 4d 6−a 6−g 6+i 6−l 6n 6p 6−s 6−t 6−u	2 4+a 4c 6−b 6c 6+g 6+j 6m 6+o 6+r 6+u 6−x	2 4+a 4b 6+b 6e 6+f 6+k 6+l 6+q 6+t 6w 6+x	2 4−a 6−f 6−i 6−j 6−v 6y
Σ27a	2 4+a 4d	1 3b 5a 5+d 5+e 5+f 5j	0 4c 6−i 6+i 6n 6p 6y	2 4−a 4b 6+a 6+f 6+g 6+j 6+l 6+s 6+t 6+u 6+v	1 5b 5−h 7+ak 7+am 7−ag 7+bi 7+bd 7+j 7+r 7+v 7+x	3b 5−e 5−f 7+af 7bf 7+bg 7b 7+bl 7−bg 7k 7u 7+w	3b 5c 5+h 7+ab 7+ae 7+ax 7+bn 7+be 7+f 7+g 7+t 7+z	3a 5g 5i 7−al 7+at 7−ar 7+az 7+bj 7+bp 7+l 7−p 7+y	1 5−d 7av 7ad 7−af 7−bl 7−w
Σ27b	2 4−a 4b 4c	1 3a 3b 5b 5c 5−d 5−e 5−f 5g 5+h 5−h 5i	2 4+a 4b 6−a 6−f 6−g 6−j 6−l 6−s 6−t 6−u 6−v	0 2 4−a 4+a 4c 4d 6+b 6−b 6c 6d 6e 6h 6−k 6+k 6m 6−o 6+o 6−q 6+q 6−r 6+r 6w 6+x 6−x	3a 3b 5+d 5+e 5g 5+h 7a 7+aw 7−aj 7−ap 7−ai 7aa 7−as 7−bh 7−bq 7br 7+bo 7−bb 7−bo 7−d 7e 7−h 7−m 7−s	1 3b 5a 5−d 5−f 5j 7−ak 7−am 7−ab 7−at 7−az 7+ag 7−ax 7−ae 7−bn 7−bj 7−bd 7−bp 7−f 7−g 7−j 7−l 7+p 7−r	1 3a 5b 5+d 5+f 5i 7an 7+ai 7−aw 7+ay 7+bh 7−bk 7−bm 7+bb 7−ba 7+bm 7−bc 7c 7+d 7+h 7−i 7−n 7o 7q	1 3b 5c 5+e 5+f 5−h 7+as 7ac 7−ay 7aq 7+aj 7+ah 7au 7−ah 7+ap 7ao 7+ba 7+bk 7+bq 7+bc 7+i 7+m 7+n 7+s	3b 5−e 5j 7+al 7+ar 7−be 7−bi 7−t 7−v 7−x 7−y 7−z
Σ81+a	3a 5+d 5+e 5j	2 4+a 4d 6+a 6+g 6−i 6+l 6n 6p 6+s 6+t 6+u	3b 5+e 5+f 7−af 7−bl 7bf 7+bg 7b 7−bg 7k 7u 7−w	1 3b 5a 5+d 5+f 5j 7+am 7+ak 7+ab 7+at 7+az 7−ag 7+ae 7+ax 7+bn 7+bd 7+bp 7+bj 7+f 7+g 7+j 7+l 7−p 7+r	4−a 4b 6+f 6+j 6+l 6+u 8+ak 8+bw 8+bv 8−cb 8+c 8+cx 8−da 8+du 8+ds 8+ex 8+ez 8+fg 8+fr 8+gg 8+g 8+gh 8+gc 8+h	0 4c 6−i 6+i 6p 6y 8−ad 8+ad 8bt 8ch 8ci 8+cq 8−cq 8+dl 8−dl 8+dz 8−dz 8−eo 8+eo 8fq 8−gj 8+gj 8r 8t	2 4−a 6+a 6+f 6+t 6+v 8+ay 8+ag 8+ai 8+as 8+bh 8+ca 8+dq 8+ea 8+ey 8+ej 8+ei 8+fw 8+ff 8+fn 8+fz 8+gd 8+m 8+p	2 4b 6+g 6+j 6+s 6+v 8+ae 8+bg 8+bj 8+by 8+bb 8+cp 8+cy 8+cu 8+dh 8+de 8−dw 8+en 8+fx 8+fj 8+fd 8+gm 8+q 8+x	4c 6+i 6n 8−at 8−al 8−bq 8−bk 8+ce 8−dc 8−dj 8−fy 8−gn
Σ81−a	3b 5c 5−f 5i	2 4b 4c 6−a 6d 6h 6+k 6+o 6+q 6+r 6−s 6−v	1 5b 5+h 7−am 7−ak 7+ag 7−bi 7−bd 7−j 7−r 7−v 7−x	3a 3b 5−d 5−e 5g 5−h 7a 7−aw 7+aj 7+ap 7aa 7+as 7+ai 7br 7+bh 7+bq 7+bo 7−bo 7+bb 7+d 7e 7+h 7+m 7+s	0 2 6c 6w 6−x 6+x 8−ap 8+ap 8bo 8cj 8−co 8+co 8−dv 8+dv 8−ec 8ek 8+ec 8es 8+ep 8−ep 8fu 8s 8+z 8−z	4+a 4b 6−f 6−j 6−l 6−u 8−ak 8−bv 8−bw 8+cb 8−c 8−cx 8+da 8−du 8−ds 8−ex 8−ez 8−fg 8−fr 8−gg 8−gc 8−gh 8−g 8−h	4+a 4c 6+b 6e 6−q 6−r 8+ac 8+aw 8+au 8+am 8+bi 8+b 8+cg 8+cc 8+dr 8+et 8+ed 8+fm 8+fk 8+fe 8+fs 8+gi 8−gl 8+k	4−a 4d 6−b 6−k 6m 6−o 8+az 8+ab 8+ah 8+bf 8+bc 8+cs 8+cr 8+cf 8+cv 8+dt 8+dm 8+em 8−eb 8−ft 8+fb 8+fi 8+gf 8+v	2 6−g 6−t 8+ao 8−ar 8−be 8−bm 8−cw 8−dk 8−dg 8−eg 8−gb
Σ81b	3b 5−e 5g 5+h	2 4−a 4c 6+b 6c 6−g 6−j 6m 6−o 6−r 6−u 6+x	3b 5c 5−h 7−ab 7−ax 7−ae 7−be 7−bn 7−f 7−g 7−t 7−z	1 3a 5b 5−d 5−f 5i 7+aw 7an 7−ai 7−ay 7−bh 7+ba 7+bc 7−bb 7+bk 7−bm 7+bm 7c 7−d 7−h 7+i 7+n 7o 7q	4−a 4c 6−b 6e 6+q 6+r 8−ac 8−am 8−aw 8−au 8−bi 8−b 8−cg 8−cc 8−dr 8−ed 8−et 8−fm 8−fe 8−fs 8−fk 8−gi 8+gl 8−k	2 4+a 6−a 6−f 6−t 6−v 8−ay 8−ag 8−as 8−ai 8−bh 8−ca 8−dq 8−ea 8−ei 8−ej 8−ey 8−fw 8−fn 8−ff 8−fz 8−gd 8−m 8−p	0 4d 6d 6+k 6−k 6w 8an 8db 8dd 8+ev 8−ev 8+fa 8−fa 8−f 8+fo 8+f 8−fo 8−ge 8+ga 8+ge 8−ga 8j 8n 8y	2 4+a 6h 6+o 6−q 6−x 8+aq 8+bx 8+bs 8−br 8+bn 8+cd 8+df 8+di 8+dn 8+eh 8+ew 8+eu 8−el 8+eq 8+er 8+fp 8+fh 8+w	4b 6−l 6−s 8−bd 8−ba 8−cl 8−ct 8−cn 8−dx 8−dy 8−fv 8−fc
Σ81c	3b 5b 5−d 5−h	2 4−a 4b 6−b 6e 6−f 6−k 6−l 6−q 6−t 6w 6−x	3a 5g 5i 7+ar 7+al 7−at 7−az 7−bp 7−bj 7−l 7+p 7−y	1 3b 5c 5−e 5−f 5+h 7−aj 7−ap 7ac 7ao 7au 7−as 7aq 7+ah 7−ah 7+ay 7−bq 7−ba 7−bc 7−bk 7−i 7−m 7−n 7−s	4+a 4d 6+b 6+k 6m 6+o 8−ab 8−az 8−ah 8−bc 8−bf 8−cs 8−cv 8−cf 8−cr 8−dm 8−dt 8+eb 8−em 8−fi 8+ft 8−fb 8−gf 8−v	2 4b 6−g 6−j 6−s 6−v 8−ae 8−bg 8−by 8−bb 8−bj 8−cu 8−cp 8−cy 8+dw 8−de 8−dh 8−en 8−fd 8−fj 8−fx 8−gm 8−q 8−x	2 4−a 6h 6−o 6+q 6+x 8−aq 8−bs 8−bn 8−bx 8+br 8−cd 8−dn 8−di 8−df 8−eh 8−ew 8−eq 8−eu 8+el 8−er 8−fp 8−fh 8−w	0 4c 6c 6d 6−r 6+r 8−ax 8+ax 8−av 8+av 8aj 8bl 8bu 8−dp 8+do 8+dp 8−do 8−ee 8e 8+ee 8gk 8−i 8+i 8o	4+a 6−a 6−u 8−aa 8−af 8+a 8−bz 8+ck 8−cm 8−cz 8−fl 8−l
Σ81d	3a 5a 5+f	2 4+a 6+f 6+i 6+j 6+v 6y	1 5+d 7av 7ad 7+af 7+bl 7+w	3b 5+e 5j 7−ar 7−al 7+bi 7+be 7+t 7+v 7+x 7+y 7+z	2 6+g 6+t 8+ar 8−ao 8+be 8+bm 8+cw 8+dg 8+dk 8+eg 8+gb	4c 6−i 6n 8+at 8+al 8+bq 8+bk 8−ce 8+dc 8+dj 8+fy 8+gn	4b 6+l 6+s 8+bd 8+ba 8+cn 8+ct 8+cl 8+dx 8+dy 8+fv 8+fc	4−a 6+a 6+u 8−a 8+af 8+aa 8+bz 8−ck 8+cz 8+cm 8+fl 8+l	0 6p 8−bp 8+bp 8d 8ef 8u

$$\Sigma_{(p_i,p_j)}\Sigma_{(p_j,p_k)} = \Sigma_{(p_i,p_k)}, \tag{15}$$

which is a groupoid composition law (it has the same form as for the hydrogen frequencies, see footnote 6). Since in general the decomposition of two Σ numbers into two products of two integers p_ip_j and p_jp_k is not uniquely reduced to the case $p_j = 1$, the composition of two Σ numbers is a multivalued function.

This rule can be applied to the $\Sigma 3^n$ values. It shows that any $\Sigma 3^m$ number can be composed with another $\Sigma 3^n$ number with $m \geq n$, by writing $\Sigma 3^m = 3^{m-i}3^i$, $\Sigma 3^n = 3^i 3^{n-i}$, and the result is 3^{m+n-2i} for any $i \in [0, n]$. This rule was already obtained in Reed *et al.* (2004, equation 14) with a demonstration based on string representations. It may be noted that this rule concerns the Σ numbers, which are only one aspect of the Σ

operators. Let us now consider the composition of the $\Sigma 3^n$ operators.

6.2. Composition of the Σ operators

As introduced in §3, the operators can be viewed as types of paths in a graph or as types of arrows in a groupoid. Both representations are suitable to calculate their composition (see also Appendix *A*).

(i) The operators $\Sigma 3^n$ can be represented by types of arrows in the groupoid $\mathbf{\Gamma}^\infty$. They define a specific misorientation between the primary crystal α^0 and a set of variants of *n*th generation, α_j^n, equivalently oriented with reference to α^0. As introduced in §4.1, a $\Sigma 3^m x$ operator can be composed with a $\Sigma 3^n y$ operator by writing $\Sigma 3^m x = \{(\alpha^0 \triangleright \alpha_i^m)\}$ and $\Sigma 3^n y = \{(\alpha_i^m \triangleright \alpha_j^{m+n})\}$ and the result is the set of operators that link the variant α^0 to the variants α_j^{m+n}: $\Sigma 3^m x \Sigma 3^n y = \{(\alpha^0 \triangleright \alpha_i^m)(\alpha_i^m \triangleright \alpha_j^{m+n})\} = \{(\alpha^0 \triangleright \alpha_j^{m+n})\} = \{\Sigma 3^q z\}$. This composition is multivalued. By determining the variants associated with each operator, the composition can be easily determined without any matrix calculation. This method has already been applied to calculate the composition of the operators that link the orientational variants generated by a structural phase transition (Cayron, 2006).

(ii) The operators $\Sigma 3^n$ can be represented by types of paths in the graph of Fig. 7. The method used to calculate their composition is the same whatever the substructure of $\mathbf{\Gamma}^\infty$ chosen for the coding ($\Sigma 3^\omega$ or $\Sigma 3^\xi$). It is based on the fact that each string in $\Sigma 3^\omega$ (or $\Sigma 3^\xi$) is equivalent to other strings of $\Sigma 3^\omega$ (or $\Sigma 3^\xi$) due to the global symmetry. The operators are elements of the quotient structure $\Sigma 3^\omega/\Re^\omega$ (or $\Sigma 3^\xi/\Re^\xi$), where $\Re^\omega$ (or $\Re^\xi$) is the equivalence relation on the strings. The composition of two operators $\Sigma 3^m x$ and $\Sigma 3^n y$, both written as sets of equivalent strings, is then easily obtained: (*a*) by choosing one string in each of the two lists, and concatenating the two strings (respecting the simplification rule of the structure), (*b*) by identifying the resulting string with an operator (which supposes that all the operators have been previously encoded up to the order $m + n$), and (*c*) by repeating the process for all the strings of the two operators. In other words, if $\Sigma 3^m x = \{s_1, \ldots, s_i, \ldots\}$ and $\Sigma 3^m y = \{t_1, \ldots, t_j, \ldots\}$, we chose $\Sigma 3^m x \ni s_i$ and $\Sigma 3^n y \ni t_j$, then $s_i t_j \in \Sigma 3^q z$, and by repeating the process $\Sigma 3^m x \Sigma 3^n y = \{\Sigma 3^q z\}$. The composition is multivalued. This method is very effective due to the highly symmetric character of the graph. We can give some examples with the two encoding structures: the $\Sigma 3^\omega$ group and the $\Sigma 3^\xi$ semigroup.

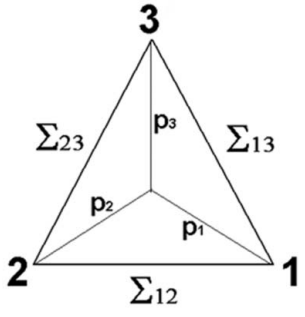

Figure 9
Schematic representation of the Σ composition rule for three crystals 1, 2 and 3 linked by misorientations for which the Σ numbers are Σ_{12}, Σ_{13} and Σ_{23}. The rule imposes that $\Sigma_{12} = p_1p_2$, $\Sigma_{23} = p_2p_3$ and $\Sigma_{13} = p_1p_3$.

6.3. Calculation with the free group $\Sigma 3^\omega$

The equivalence of the four fractal branches imposes that the letters *a*, *b*, *c*, *d* used in the free group $\Sigma 3^\omega$ are equivalent. These letters can be permuted in the strings. For example, the string *aca* is equivalent to the string *dbd* by the permutation $(a, b, c, d) \rightarrow (d, c, b, a)$. Both strings belong to the same operator. Each operator is encoded by a set of equivalent strings. For example, the operator $\Sigma 3 = \{a, b, c, d\}$ and the operator $\Sigma 27a = \{aba, aca, ada, bab, bcb, bdb, cac, cbc, cdc, dad, dbd, dcd\}$. The composition of the operators is obtained by concatenation and by applying the simplification rule $ii = \emptyset$ for $i \in \{a, b, c, d\}$. It gives $\Sigma 27a \Sigma 3 = \{ab, ac, ad, abab, acab, adab, abac, acac, adac, abad, acad, adad, \ldots\} = \{\Sigma 9, \Sigma 81+a, \Sigma 81d\}$.

6.4. Calculation with the semigroup $\Sigma 3^\xi$

The threefold symmetry of each fractal branch imposes that the indices 1, 2, 3 in the semigroup $\Sigma 3^\xi$ are equivalent and can therefore be permuted in the strings. Moreover, owing to the equivalence of the four branches of the fractal, each string of kind $ijk \ldots l$ is equivalent to a string of kind $0jk \ldots l$. Here again, an operator is a set of equivalent strings. For example, the operator $\Sigma 3 = \{0, 1, 2, 3\}$ and the operator $\Sigma 27a = \{111, 222, 333, 211, 311, 122, 322, 133, 233, 011, 022, 033\}$. The composition of the operators is obtained by concatenation and by applying the simplification rule (10). It gives $\Sigma 27a\ \Sigma 3 = \{11, 1111, 1112, \ldots\} = \{\Sigma 9, \Sigma 81+a, \Sigma 81d\}$. One may observe that the result is the same as that obtained with the $\Sigma 3^\omega$ group.

The $\Sigma 3^m x \Sigma 3^n y$ composition table for $m \leq 4$ and $n \leq 4$ can be determined using the $\Sigma 3^\xi$ coding in a few seconds using a modern desktop computer, and is reported in Table 3 (the tables for higher orders are available on demand). The composition is multivalued due to the groupoid structure of $\mathbf{\Gamma}^\infty$. The table is asymmetric because of the non-commutativity of the operators. It can be forced to be symmetric by ignoring the signs of the polar operators, but this would lead to lost information. We will now explain the practical importance of such a table in metallurgy.

7. Application for the identification of $\Sigma 3^n$ grain boundaries

Many defects in metals and alloys are formed in grain boundaries. The study of their local crystallographic environment can bring new understanding of their formation. Are the defects in twinned materials situated in random grain boundaries or in the special $\Sigma 3^n$ grain boundaries? The response is not always obvious because it is difficult to distinguish a random misorientation from a $\Sigma 3^n$ operator with high order *n*. Indeed, the $\Sigma 3^n$ operators are numerous and

nearly homogeneously distributed in space for twinning order $n \geq 5$ (see Fig. 8). The identification of the $\Sigma 3^n$ grain boundaries is also a key point used to reconstruct the twin-related domains. As introduced in §1, the TRD size is an important microstructural parameter and many engineers try to improve the mechanical properties by optimizing the elaboration processes in order to produce structures with large TRDs. The determination of the TRDs by EBSD could be a useful aid for these engineering developments. Very often, the TRDs can be easily identified by following the connected paths (*i.e.* chains) of Σ3 boundaries between the grains. However, such a method is not always possible. Indeed, in some architectured materials with low dimensionality, the Σ3 chains that link the grains of the TRDs are not at the sample surface but situated under the surface and their locations make their direct identification impossible with the EBSD technique (which is a surface technique). We give some engineering examples to show how the composition Table 3 helps to solve these metallurgical problems. The EBSD maps have been acquired on a LEO-1530 SEM equipped with a Nordlys II CCD camera and have been analysed using the *Channel5* software (HKL Technology).

7.1. Local environment of a void on a copper line

In microelectronic devices, the reduction of the width of the copper interconnection lines and the use of new barrier and capping layers have led to some new reliability problems. The stress concentrations during the elaboration processes sometimes lead to the formation of voids that can grow and completely damage the lines, this type of defect is called stress-induced voiding (SIV) (Børgesen *et al.*, 1992; Shao *et al.*, 2006). Some relations exist between the global texture and the SIV (Nucci, 1997; Sekiguchi *et al.*, 2003), but the coupling mechanisms between the stresses, the atom migration and the local crystallographic environment remain poorly understood. Local EBSD analyses could help in the understanding of these mechanisms.

In Fig. 10, a stress-induced void has been localized in a copper line. It is situated inside a TRD (here clearly identifiable by the Σ3 chains between the grains) in a boundary between four grains (denoted 1, 2, 3 and 4). This TRD has been reconstructed by ignoring the Σ3 grain boundaries, *i.e.* the same colour has been attributed to the grains separated by a Σ3 grain boundary. The misorientations between these grains are $R_{21} = (28.4^\circ, [2\bar{1}\bar{4}])$, $R_{23} = (59.8^\circ, [\bar{1}\bar{1}1])$, $R_{34} = (35.9^\circ, [2\bar{1}0])$, $R_{41} = (38.4^\circ, [\bar{1}0\bar{1}])$, $R_{13} = (48.9^\circ, [\bar{1}\bar{4}4])$ and $R_{24} = (38.7^\circ, [\bar{2}41])$. Three of them are easy to index: $R_{23} = \Sigma 3$, $R_{34} = \Sigma 27b$ and $R_{41} = \Sigma 9$, but the three others correspond to higher twinning orders and are more difficult to identify. We determine the maximum possible twinning order by counting the number of Σ3 in the shorter Σ3 chain that links two grains. Then, we identify some possible solutions by looking at Table 2 (rotation angles and axes). Three solutions are possible for R_{24} = (Σ81+a, Σ81−*a* or Σ81b), two for R_{13} = ($\Sigma 3^5$+h or $\Sigma 3^5$−h), and four for R_{12} = ($\Sigma 3^6$+f, $\Sigma 3^6$−f, $\Sigma 3^6$+g or $\Sigma 3^6$−g). Moreover, $R_{21} = R_{24}R_{41}$ = (Σ81+aΣ9, Σ81−aΣ9 or Σ81bΣ9), and if one looks at the results of these compositions in Table 3 and compares them with the possible solutions already identified from the EBSD map ($\Sigma 3^6$+f, $\Sigma 3^6$−f, $\Sigma 3^6$+g or $\Sigma 3^6$−g),

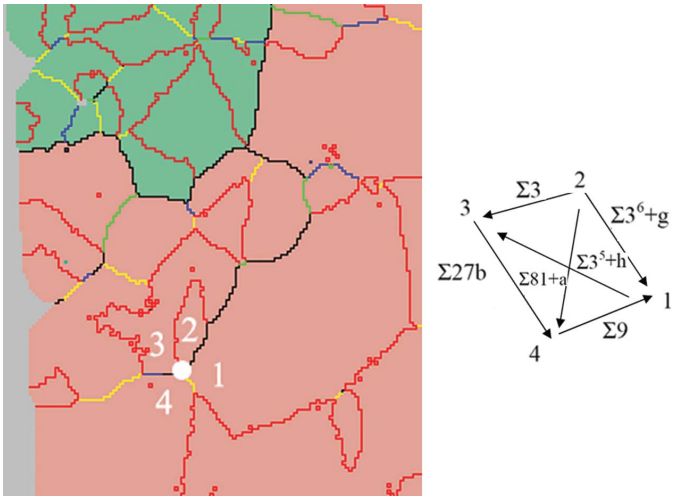

Figure 10
EBSD map around a void (the white disc) situated at the junction of four grains. In the figure, the Σ3 boundaries are in red, the Σ9 in yellow, the Σ27 in blue and the Σ81 in green. The higher-order $\Sigma 3^n$ with $n \geq 5$ and the 'random' boundaries are in black. The grains around the void are linked by the following rotations: $R_{21} = (28.4^\circ, [2\bar{1}\bar{4}])$, $R_{23} = (59.8^\circ, [\bar{1}\bar{1}1])$, $R_{34} = (35.9^\circ, [2\bar{1}0])$, $R_{41} = (38.4^\circ, [\bar{1}0\bar{1}])$, $R_{13} = (48.9^\circ, [\bar{1}\bar{4}4])$ and $R_{24} = (38.7^\circ, [\bar{2}41])$. The rotation angles and axes are given by the *Channel5* software (the reported axes are not the true ones but axes with indices lower than 10 and close to the true ones with a tolerance angle of 5°). The identification of these experimental rotations to some $\Sigma 3^n$ operators requires the use of the groupoid composition Table 3.

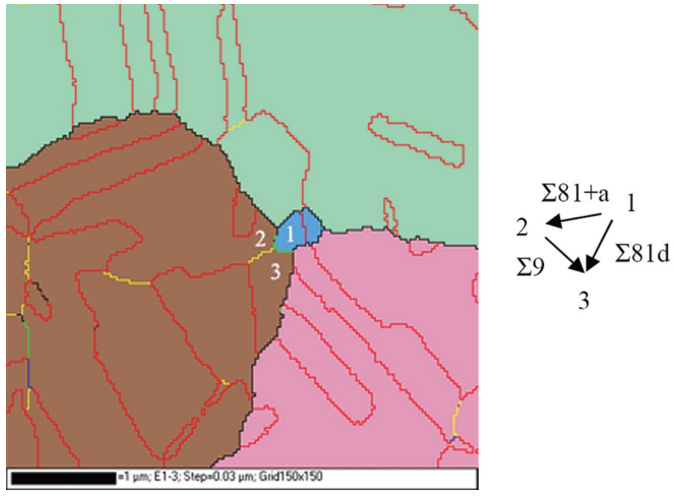

Figure 11
EBSD map around a hillock situated at the junction of three TRDs (reconstructed by ignoring only the Σ3 and Σ9 boundaries). The conventions for the colours of the boundaries are the same as that of Fig. 10. The hillock (at the centre of the figure, in blue) is connected to the left TRD (in brown) by two misorientations that form a triple junction constituted by the rotations $R_{12} = (38.7^\circ, [4\bar{1}3])$, $R_{23} = (39.3^\circ, [101])$ and $R_{13} = (59.1^\circ, [434])$. These are close to the Σ81+a, Σ9 and Σ81d operators, respectively. Their composition verifies the groupoid composition Table 3. We conclude that the hillock is a twinned branch of the left TRD and not a new nucleated TRD.

one may check that the only solution is R_{24} = Σ81+a and R_{21} = $\Sigma3^6$+g. This result could also have been obtained by considering $R_{21} = R_{23}R_{31}$ = (Σ3$\Sigma3^5$+h or Σ3$\Sigma3^5$−h) = ({$\Sigma3^6$+l, $\Sigma3^6$+b, $\Sigma3^6$e, $\Sigma3^4$c} or {$\Sigma3^6$+g, $\Sigma3^6$c, $\Sigma3^6$−x, $\Sigma3^4$b}) (not presented in Table 3 for space reasons), which leads to the same unique solution R_{21} = $\Sigma3^6$+g. This example is very interesting because it proves that it is sometimes possible to unambiguously identify the $\Sigma3^n$ grain boundaries for orders $n \geq 6$ and that the distinction between direct and inverse polar operators is important for the identification method.

7.2. Local environment of a hillock on a copper film

Hillocks are defects that may appear in the interconnection lines of electronic devices during the elaboration process or by electromigration damage. Wei *et al.* (2002) believe that these are likely to be new nucleated grains, whereas Gladkikh *et al.* (1995) believe that they result from the growth of a neighbouring grain. Let us now consider the hillock on a copper film shown in the EBSD map in Fig. 11. The TRDs were reconstructed by neglecting only the Σ3 and Σ9 special boundaries. At first glance, the hillock appears as a new nucleated TRD. Indeed, there is no Σ3 chain between it and any grain of the three TRDs. However, if we consider the $\Sigma3^n$ operators at higher orders, the hillock seems to be linked to the left TRD by two misorientations close to Σ81 forming a triple junction R_{12} = Σ81+a, R_{23} = Σ9 and R_{13} = Σ81d. Are these misorientations close to the $\Sigma3^n$ operators 'by accident' and in fact 'random'? A way to be more confident is to check the coherency of the triple junction, *i.e.* to check that their composition is in agreement with the theoretical composition Table 3. The verification is done because $R_{12}R_{23}$ = Σ81+aΣ9 = {$\Sigma3^2$, $\Sigma3^4$+a, $\Sigma3^4$d, $\Sigma3^6$+a, $\Sigma3^6$+g, $\Sigma3^6$−i, $\Sigma3^6$+l, $\Sigma3^6$n, $\Sigma3^6$p, $\Sigma3^6$+s, $\Sigma3^6$+t, $\Sigma3^6$+u} ∋ Σ81d = R_{13}. This verification reinforces the probability that the hillock is in fact a multiply twinned branch of the left TRD, and its formation should imply a growth mechanism (with twinning) without nucleation. A deeper statistical study is required to quantify these probabilities as a function of the tolerance angles. The calculations could be based on the generation of triplets of randomly oriented crystals following a method introduced in Cayron *et al.* (2006).

7.3. Application to the reconstruction of TRDs in narrow copper lines

The Σ3 twins have in general an electrical resistivity one decade lower than that of the conventional high-angle grain boundaries [and the least resistive Σ3 boundaries are those with {111} boundary planes, see Sutton & Balluffi (1995)]. Therefore, some engineering teams increase the size of the TRDs in the interconnection Cu lines to reduce their resistivity.[14] In parallel, some EBSD characterization studies try to reconstruct the TRDs in order to correlate their mean size to the electric measurements. However, this reconstruction is usually performed by neglecting only the Σ3 boundaries (Mirpuri & Szpunar, 2004), which gives undervalued results for narrow lines. Indeed, when the lines are narrow (<1 µm), they often have a 'bamboo-like' structure (the grains have the same width as the lines), as shown in Fig. 12. Then, although there is always a Σ3 chain between two grains of a TRD, this chain is not always situated at the surface of the sample and becomes invisible in the EBSD maps. When this situation occurs, these grains seem to be separated by a $\Sigma3^n$ boundary with $n \geq 2$ in EBSD, but one must remember that they are in fact connected by a Σ3 chain of grains located under the surface which acts as a low resistivity path between these two grains. Therefore, all the 'reasonable' twinning orders n of the $\Sigma3^n$ boundaries should be considered to reconstruct satisfactorily the TRDs. And considering the Σ9 in addition to the Σ3 boundaries is far from enough. On the copper lines represented in Fig. 12, some TRDs have been reconstructed by neglecting only the Σ3 and Σ9 boundaries. We have identified many grain boundaries separating these partial TRDs that are of type $\Sigma3^n$ with $n \geq 3$ and that verify Table 3. One frontier is presented in the square on the bottom left of the figure. It is constituted of $\Sigma3^n$ boundaries: R_{23} = Σ3, R_{31} = Σ81b and R_{21} = $\Sigma3^5$g. Such a junction is coherent with Table 3 because it respects $R_{23}R_{31}$ = Σ3Σ81b = {$\Sigma3^3$b, $\Sigma3^5$+e, $\Sigma3^5$g, $\Sigma3^5$−h} ∋ $\Sigma3^5$g = R_{21}. Therefore, the two TRDs in the square of Fig. 12 are in fact only one TRD. In a first analysis, for narrow copper lines with a 'bamboo-like' structure, we estimate that the TRD mean size calculated by neglecting only the Σ3 boundaries (and not the $\Sigma3^n$ ones with $n \geq 2$) is at least 50% undervalued.

Once a TRD is reconstructed, it may be checked that its corresponding pole figure is in agreement with the simulations of Fig. 8. In some cases, some missing dots can bring useful

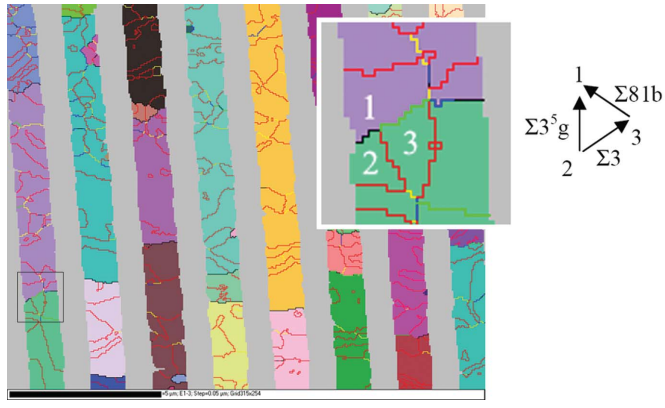

Figure 12
EBSD map of copper lines with a 'bamboo-like' structure. The conventions for the colours of the boundaries are the same as that of Fig. 10. The TRDs are reconstructed by ignoring only the Σ3 and Σ9 boundaries. The two 'assumed' TRDs in purple and green in the square on the bottom left part of the image (reported with higher magnification in the upper right part of the figure) are separated by Σ81 and higher-order $\Sigma3^n$ operators. For one part of the boundary, the rotations are R_{23} = (59.3°, [$\bar{1}$10]), R_{31} = (38.1°, [$\bar{1}$4$\bar{1}$]) and R_{21} = (43.2°, [4$\bar{1}\bar{1}$]). These are close to the Σ3, Σ81b and $\Sigma3^5$g operators, respectively. Their composition verifies the groupoid composition Table 3. The same verification was done along the whole boundary. We conclude that these two TRDs are in fact only one TRD.

[14] For example, it is possible to elaborate nano-twinned copper foils with ultrahigh strength and low electrical resistivity (Lu *et al.*, 2004).

information about a variant selection mechanism during the recrystallization. For instance, the experimental pole figure of a TRD reconstructed in a copper film and oriented in the [111] direction of the primary crystal is reported in Fig. 13(*a*); its comparison to the theoretical pole Fig. 13(*b*) proves that the twinning order of this TRD is $n = 2$ and that one main branch of the fractal is missing [the fractal is constituted of only three branches, such as the ones visible in Fig. 3(*a*)]. More thorough analysis would be required to know if the fourth branch is missing or if it is situated below the surface.

8. Conclusions

The idea of a groupoid has been introduced. Three types of groupoid elements have been described: the objects, the operations (also called arrows) between these objects and the operators that are types of operations (they are written as sets of equivalent operations).

An assembly constituted of one crystal with its four twinned variants can be represented by a groupoid $\mathbf{\Gamma}^{(0+1)}$. More generally, an assembly of multiply twinned crystals linked by $\Sigma 3^n$ operators with $n \in \mathbb{N}$ can be represented geometrically by a three-dimensional fractal and algebraically by the groupoid $\mathbf{\Gamma}^{\infty} = \mathbf{\Gamma}^{(0+1+\ldots+n)}$ with $n \rightarrow \infty$. The algebraic details of $\mathbf{\Gamma}^{\infty}$ were not studied but symmetry considerations on the three-dimensional fractal have allowed us to determine some of its properties. For example, the general formulae giving the number of variants and the number of operators as functions of the twinning order n were established. The $\Sigma 3^{\omega}$ free group introduced by Reed *et al.* (2004) is a substructure of $\mathbf{\Gamma}^{\infty}$. Other substructures can be used. For example, we have introduced the $\Sigma 3^{\xi}$ semigroup that leads to a different coding (with a different simplification rule), but to a two-dimensional fractal graph similar to the one that could be obtained with the $\Sigma 3^{\omega}$ free group. Whatever the substructure we use for the coding ($\Sigma 3^{\omega}$ or $\Sigma 3^{\xi}$), the $\Sigma 3^n$ operators can be written as sets of equivalent strings. The composition of two operators can then be easily determined without any matrix calculation by concatenating all the couples of strings chosen in their respective set and by applying the simplification rule of the substructure. The composition of operators is multivalued. This property can be understood by taking into consideration that the general structure of multiple twinning is a groupoid and not simply a group. The composition table has been reported for orders $n \leq 4$ (and was determined at higher orders).

Some metallurgical examples were given showing how this table could be used in EBSD for a better identification of the local crystallographic environment of some defects in multiply twinned materials or for improving the reconstruction of the TRDs. We have stressed that the distinction between polar and ambivalent $\Sigma 3^n$ operators is important in the identification method. The approach we have followed is general and can be used to compute an automatic recognition of the $\Sigma 3^n$ grain boundaries and an automatic reconstruction of the TRDs.

The present study can be applied to treat multiple twinning in non-cubic materials because it is not based on quaternions. However, the general theory treating any series of cycles of phase transitions remains to be established. The answer is probably to be found in algebraic structures more elaborated than groupoids such as the cohomology of groupoids (Connes, 1990). This research will require the help of mathematicians.

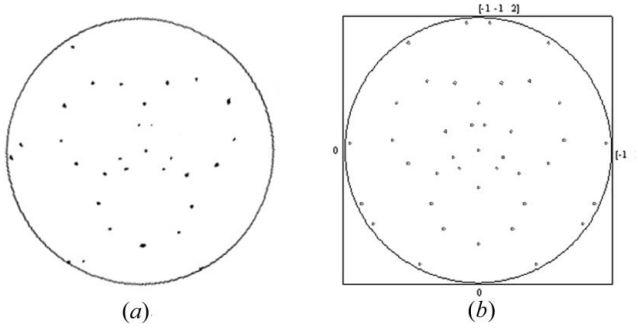

Figure 13
Comparison between (*a*) an experimental pole figure of a TRD observed by EBSD in a copper film with a primary crystal oriented with [111]//*z*, where *z* is the normal to the sample surface, and (*b*) a theoretical pole figure of an assembly of multiply twinned crystals with $n \leq 2$. In this simulation, only three of the four branches have been considered (branch 0 would give many spots that do not appear in the experimental pattern). Some theoretical variants of order $n = 2$ are also absent (they correspond to the differences between the theoretical and experimental patterns).

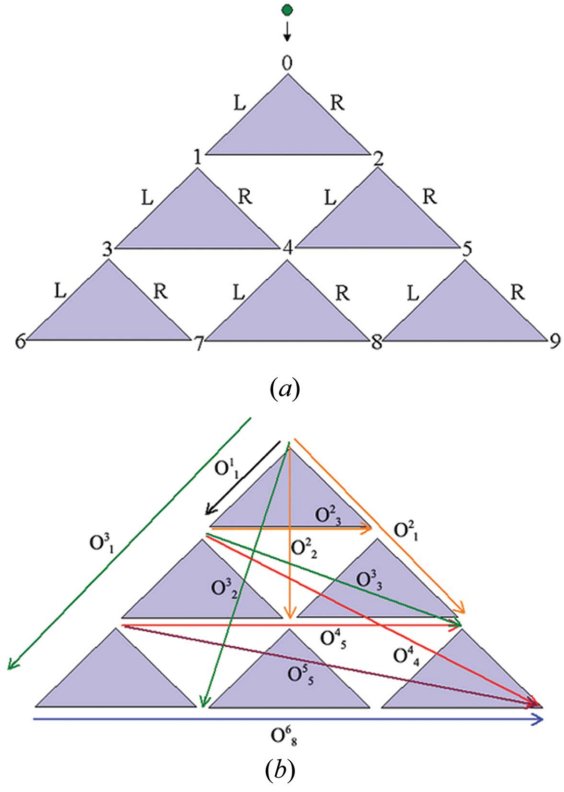

Figure 14
(*a*) Structure built from isosceles triangles. (*b*) The different types of paths of a ball moving between the triangles are the operators of a groupoid.

To conclude, we would like to encourage crystallographers interested in phase transitions, quasicrystals or other problems involving partial symmetries to consider groupoids as a very useful algebraic tool that advantageously enlarges the idea of groups.

APPENDIX *A*

In this Appendix, we present a simple non-crystallographic geometrical case, with local and global symmetries, in order to clarify the idea of 'operator' and its link with the groupoids. Let us imagine a ball moving on a flat surface in a structure constituted by isosceles triangles that have vertical mirror symmetry (Fig. 14). How can we encode the different movements of the ball on such a structure?

A1. Operators viewed as types of paths in a graph

One may notice that the ball has five possibilities at each vertex: left or right while going to the bottom (L or R), left or right while going to the top (L^{-1}, R^{-1}), or coming to rest (denoted $\emptyset$). This classification of possibilities is due to the local symmetries of the structure. Of course, it can be created a free group $\mathbf{G}^{\infty}$ constituted by the letters L, R, L^{-1} and R^{-1} and all the infinite combinations of these letters.[15] The corresponding infinite graph would be similar to Fig. 14(*a*), imagined to be repeated an infinity of times. Any trajectory of the ball is represented by a string of the free group $\mathbf{G}^{\infty}$. But there are two problems with such a representation: (*a*) such a group is infinite whereas Fig. 14(*a*) is finite, and (*b*) in such a graph the local and global symmetries are not represented. Indeed, one may assume that different trajectories are of the same type due to the local symmetries of the structure. From Fig. 14(*a*), we can effectively notice that two strings are equivalent by

$$\text{global permutation:} \quad (\mathrm{L}, \mathrm{R}, \mathrm{L}^{-1}, \mathrm{R}^{-1}) \rightarrow (\mathrm{R}, \mathrm{L}, \mathrm{R}^{-1}, \mathrm{L}^{-1}) \tag{16}$$

$$\text{partial commutativity:} \quad \mathrm{LR} = \mathrm{RL} \tag{17}$$

$$\text{partial commutativity:} \quad \mathrm{LR}^{-1} = \mathrm{R}^{-1}\mathrm{L}. \tag{18}$$

The rule (16) is the algebraic expression of the global vertical mirror symmetry. Conditions (17) and (18) are the algebraic expressions of the local vertical mirror symmetries.[16] These rules allow the creation of an equivalence relation $\Re$ on the different trajectories of the ball. The distinct types of trajectories are given by the elements of the quotient set $\mathbf{G}^{\infty}/\Re$. There is no reason for $\mathbf{G}^{\infty}/\Re$ to be a group, and in fact this structure appears to be quite complex. We propose in the following a method to define its elements and their compositions.

Owing to the local vertical mirror symmetry, the actions L and R are equivalent; there is no way to predict that the ball will move to the left or to the right. One may then accept that the action 'moving down' on the structure of Fig. 14 is not a classical application, but a bivalued function that we will denote $O_1^1(x) = \{\mathrm{L}, \mathrm{R}\}$, for any position x of the ball on the structure. Similarly, the action 'moving up' is denoted $O_1^{1\,-1} = \{\mathrm{L}^{-1}, \mathrm{R}^{-1}\}$. The operator 'coming to rest' is $O_0^1 = \emptyset$. These three operators will be called operators of first generation. For the second generation, the operators are $O_0^2 = O_0^1 = \{\mathrm{LL}^{-1}, \mathrm{RR}^{-1}, \mathrm{R}^{-1}\mathrm{R}, \mathrm{L}^{-1}\mathrm{L}\} = \emptyset$, $O_1^2 = \{\mathrm{LL}, \mathrm{RR}\}$, $O_2^2 = \{\mathrm{LR}, \mathrm{RL}\}$, $O_3^2 = O_3^{2\,-1} = \{\mathrm{L}^{-1}\mathrm{R}, \mathrm{R}^{-1}\mathrm{L}, \mathrm{LR}^{-1}, \mathrm{RL}^{-1}\}$, $O_1^{2\,-1} = \{\mathrm{L}^{-1}\mathrm{L}^{-1}, \mathrm{R}^{-1}\mathrm{R}^{-1}\}$ and $O_2^{2\,-1} = \{\mathrm{L}^{-1}\mathrm{R}^{-1}, \mathrm{R}^{-1}\mathrm{L}^{-1}\}$. For the third generation, the new operators are $O_1^3 = \{\mathrm{LLL}, \mathrm{RRR}\}$, $O_2^3 = \{\mathrm{LRR}, \mathrm{RLR}, \mathrm{LRL}, \mathrm{RLL}, \mathrm{RRL}, \mathrm{LLR}\}$, $O_3^3 = \{\mathrm{LR}^{-1}\mathrm{L}, \mathrm{RL}^{-1}\mathrm{R}, \mathrm{R}^{-1}\mathrm{LL}, \mathrm{LLR}^{-1}, \mathrm{L}^{-1}\mathrm{RR}, \mathrm{RRL}^{-1}\}$ and their inverses (which are all distinct). These operators are represented in Fig. 14(*b*). More generally, one can form the operators of order n, O_j^n, by forming all the strings with n letters in the set $\{\mathrm{L}, \mathrm{R}, \mathrm{L}^{-1}, \mathrm{R}^{-1}\}$ and finding the strings that are equivalent by the conditions (16), (17) and (18). The operators are the elements of $\mathbf{G}^{\infty}/\Re$. Two operators O_i^m and O_j^n can also be composed: (i) by choosing on the left a string of O_i^m and on the right a string of O_j^n and concatenating them; (ii) by identifying the resulting string to an operator of order $\leq m+n$; and (iii) by repeating this process for all the couples of strings in (O_i^m, O_j^n). For example, $O_1^1 O_1^1 = \{\mathrm{LL}, \mathrm{RR}, \mathrm{RL}, \mathrm{LR}\} = \{O_1^2, O_2^2\}$, $O_1^{1\,-1} O_1^1 = \{\emptyset, \mathrm{L}^{-1}\mathrm{R}, \mathrm{R}^{-1}\mathrm{L}\} = \{O_0^2, O_3^2\}$, $O_1^{1\,-1} O_1^2 = \{\mathrm{L}, \mathrm{L}^{-1}\mathrm{RR}, \mathrm{R}^{-1}\mathrm{LL}, \mathrm{R}\} = \{O_1^1, O_3^3\}$. From these examples, the composition of operators (*i.e.* types of trajectories, *i.e.* elements of $\mathbf{G}^{\infty}/\Re$) appears to be multivalued. Some readers may be shocked by the use of a multivalued composition; a way to accept it is to realize that such a composition naturally results from an underlying groupoid structure.

A2. Operators viewed as types of arrows in a groupoid

In the previous paragraph, we have voluntarily ignored the positions x on which the operations were applied (denoted as 0 to 9 in Fig. 14*a*). A pair of positions, denoted $(x \triangleright y)$, can be viewed as an arrow from x to y. The arrows form a pair groupoid. The composition law is $(x \triangleright y)(y \triangleright z) = (x \triangleright z)$ and each arrow has an inverse given by $(x \triangleright y)^{-1} = (y \triangleright x)$. The operators appear as types of arrows. For example, $O_1^1 = \{(0 \triangleright 1), (0 \triangleright 2), (1 \triangleright 3), (1 \triangleright 4), (2 \triangleright 4), (2 \triangleright 5), (3 \triangleright 6), (3 \triangleright 7), (4 \triangleright 7), (4 \triangleright 8), (5 \triangleright 8), (5 \triangleright 9)\}$. The operator $O_1^{1\,-1}$ is constituted by the inverse arrows, and O_0^1 by the arrows of type $(i \triangleright i)$ for $i \in [0, 9]$. It can also be noticed that $O_1^2 = \{(0 \triangleright 3), (0 \triangleright 5), (1 \triangleright 8), (2 \triangleright 7), (1 \triangleright 6), (2 \triangleright 9)\}$ and $O_2^2 = \{(0 \triangleright 4), (1 \triangleright 7), (2 \triangleright 8)\}$. Here, the different arrows constituting the operators are geometrically obvious. Generally, they can be found by expressing the local symmetries. In the present example, one could use the vertical mirror symmetry that is the permutation $(0, 1, 2, 3, 4, 5, 6, 7, 8, 9) \rightarrow (0, 2, 1, 5, 4, 3, 9, 8, 7, 6)$ and the translations that put in correspondence some points of the structure, for example the translation $(0 \triangleright 1)$ expressed by the

[15] If Fig. 14 is imagined as a ball falling on the structure, the gravity field imposes a temporal arrow on the process, then the reverse actions are not allowed (the ball is always moving down) and we should use a free semigroup structure.

[16] If L^{-1} and R^{-1} are imagined as the reverse actions of L and R obtained by a time inversion, condition (18) becomes more subtle: the left and the right directions are exchanged when the time is reversed.

order		n	0	1		2			3			
	↗		O_0	O_1^1		O_1^2		O_2^2	O_1^3		O_2^3	
m		y / x	0	1	2	3	5	4	6	9	7	8
0	O_0	0	O_0	O_1^1	O_1^1	O_1^2	O_1^2	O_2^2	O_1^3	O_1^3	O_2^3	O_2^3
1	O_1^1	1	O_1^{-1}	O_0	O_3^2	O_1^1	O_3^3	O_1^1	O_1^2	O_4^4	O_2^2	O_1^2
		2	O_1^{-1}	O_3^2	O_0	O_3^3	O_1^1	O_1^1	O_4^4	O_1^2	O_1^2	O_2^2
2	O_1^2	3	O_1^{-2}	O_1^{-1}	O_3^{-3}	O_0	O_5^4	O_3^2	O_1^1	O_5^5	O_1^1	O_3^3
		5	O_1^{-2}	O_3^{-3}	O_1^{-1}	O_5^4	O_0	O_3^2	O_5^5	O_1^1	O_3^3	O_1^1
	O_2^2	4	O_2^{-2}	O_1^{-1}	O_1^{-1}	O_3^{-2}	O_3^{-2}	O_0	O_3^3	O_3^3	O_1^1	O_1^1
3	O_1^3	6	O_1^{-3}	O_1^{-2}	O_4^{-4}	O_1^{-1}	O_5^{-5}	O_3^{-3}	O_0	O_8^6	O_3^2	O_5^4
		9	O_1^{-3}	O_4^{-4}	O_1^{-2}	O_5^{-5}	O_1^{-1}	O_3^{-3}	O_8^6	O_0	O_5^4	O_3^2
	O_2^3	7	O_2^{-3}	O_2^{-2}	O_1^{-2}	O_1^{-1}	O_5^{-3}	O_1^{-1}	O_3^2	O_5^4	O_0	O_3^2
		8	O_2^{-3}	O_1^{-2}	O_2^{-2}	O_3^{-3}	O_1^{-1}	O_1^{-1}	O_5^4	O_5^2	O_3^2	O_0

Figure 15
Composition table ($O_i^m, O_j^n \rightarrow O_i^{m-1}O_j^n$) corresponding to Fig. 14. The objects (x or y) are the positions of the ball. The position 0 is used as a reference position. The arrows ($0 \triangleright x$) are in columns and they are reassembled into operators. The arrows ($0 \triangleright y$) are in lines and they are reassembled into operators. The composition of arrows is performed by determining $(0 \triangleright x)^{-1}$ $(0 \triangleright y) = (x \triangleright y)$. The different resulting arrows are expressed by their operators. For more simplicity, the inverse of a polar operator is denoted $O_i^{m-1} = O_i^{-m}$. The composition is multivalued.

application (0, 1, 2, 3, 4, 5, 6, 7, 8, 9) → (1, 3, 4, 6, 7, 8, ø, ø, ø, ø), where ø means 'no image'. Two operators O_i^m and O_j^n can be composed: (i) by choosing on the left one arrow of type $(x \triangleright y)$ in O_i^m and on the right one arrow of type $(y \triangleright z)$ in O_j^n; (ii) by identifying the resulting arrow $(x \triangleright z)$ with an operator; and (iii) by repeating this process for all the couples of strings in (O_i^m, O_j^n). For example, $O_1^1O_1^1 = \{(0 \triangleright 1)(1 \triangleright 3) = (0 \triangleright 3), (0 \triangleright 1)(1 \triangleright 4) = (0 \triangleright 4)$ *etc.*$\} = \{O_1^2, O_2^2\}$. One can also calculate the composition $O_i^{m-1}O_j^n$ by choosing a reference position (for example $y = 0$). Then we determine all the arrows of type $(x \triangleright z)$ by choosing one arrow of type $(0 \triangleright x)^{-1} = (x \triangleright 0)$ in O_i^{m-1} on the left and one arrow of type $(0 \triangleright z)$ in O_j^n on the right. This method has the advantage of representing the objects, the operators and their composition in the same table. The geometrical structure of Fig. 14 can then be algebraically written in a unique groupoid composition table (Fig. 15), which can be viewed as a generalization of the composition table of groups.

In this example, we have seen that, due to the local symmetries, there exist some types of paths or arrows that we have called operators. These operators can be written as sets of equivalent strings in a graph or as sets of equivalent arrows in a groupoid. They can be composed by string concatenation (in a graph) or by respecting the composition law between the arrows (in a groupoid). Whatever we choose as the method, this composition is multivalued. Composition tables can be calculated. Graphs and strings are very effective for high symmetric problems; groupoids and arrows are less effective but more general and can be applied to less symmetric problems. For example, it would be the same formalism if some isosceles triangles in Fig. 14 were suppressed or if they were changed by equilateral triangles.

We acknowledge P. Dumont-Girard (ST Microelectronics) for providing the Cu films, and L. Arnaud and J. F. Guillaumond (CEA-LETI) for the samples with the Cu lines. The fractals have been computed in Python language and represented in three dimensions thanks to the engine *Soya*. Both are freeware available on the Internet. We also acknowledge S. Zapata and D. Cooper (CEA-LETI) for helping with the English language. This study was partially supported by the French government programmes Stressnet and Cristal.

References

Andreeva, A. V. & Firsova, A. A. (1996). *Mater. Sci. Forum*, **207–209**, 189–192.
Børgesen, P., Lee, J. K., Gleixner, R. & Li, C. Y. (1992). *Appl. Phys. Lett.* **60**, 1706–1708.
Brandt, W. (1926). *Math. Ann.* **96**, 360–366.
Brown, R. (1987). *Bull. London Math. Soc.* **19**, 113–134.
Burt, J. L., Elechiguerra, J. L., Reyes-Gasga J., Montejano-Carrizales, J. M. & Jose-Yacaman, M. (2005). *J. Cryst. Growth*, **285**, 681–691.
Cayron, C. (2006). *Acta Cryst.* A**62**, 21–40.
Cayron, C., Artaud, B. & Briottet, L. (2006). *Mater. Charact.* **57**, 386–401.
Cheng, Y. (1994). *J. Phys. D: Appl. Phys.* **27**, 1938–1945.
Connes, A. (1990). *Géométrie Non Commutative*, pp. 9–22. Inter Editions, Paris.
Dornberger-Schiff, K. & Grell-Niemann, H. (1961). *Acta Cryst.* **14**, 167–177.
Fichtner, K. (1986). *Comput. Maths Applic.* **12B**, 751–762.
Friedel, G. (1904). *Étude sur les Groupements Cristallins.* Extrait du *Bullettin de la Société de l'Industrie Minérale*, Quatrième Série, Tomes III e IV. Saint-Étienne: Société de l'Imprimerie Thèolier J. Thomas et C.
Gertsman, V. Y. (2001*a*). *Acta Cryst.* A**57**, 369–377.
Gertsman, V. Y. (2001*b*). *Acta Cryst.* A**57**, 649–655.
Gertsman, V. Y. & Henager, C. H. Jr (2003). *Interface Sci.* **11**, 403–415.
Gladkikh, A., Lereah, Y., Glickman, E., Karpovski, M., Palevski, A. & Schubert, J. (1995). *Appl. Phys. Lett.* **66**, 1214–1215.
Gottstein, G. (1984). *Acta Metall.* **32**, 1117–1138.
Grimmer, H. (1974). *Acta Cryst.* A**30**, 685–688.
Grimmer, H. (1976). *Acta Cryst.* A**32**, 783–785.
Grimmer, H., Bollmann, W. & Warrington, D. H. (1974). *Acta Cryst.* A**30**, 197–207.
Grimmer, H. & Nespolo, M. (2006). *Z. Kristallogr.* **221**, 28–50.
Hahn, Th., Janovec, V. & Klapper, H. (1999). *Ferroelectrics*, **222**, 11–21.
Hahn, Th. & Klapper, H. (2003). *Twinning of Crystals. International Tables for Crystallography*, Vol. D, edited by A. Authier, pp. 393–448. Dordrecht: Kluwer Academic Publishers.
Janovec, V. (1972). *Czech. J. Phys. B*, **22**, 974–994.
Janovec, V. (1976). *Ferroelectrics*, **12**, 43–53.
Janovec, V., Hahn, Th. & Klapper H. (2003). *International Tables for Crystallography*, Vol. D, edited by A. Authier, Section 3.2, pp. 377–391. Dordrecht: Kluwer Academic Publishers.
Janovec, V. & Přívratská, J. (2003). *International Tables for Crystallography*, Vol. D, edited by A. Authier, Section 3.4, pp. 349–505. Dordrecht: Kluwer Academic Publishers.
Kopezky, Ch. V., Andreeva, A. V. & Sukhomlin, G. D. (1991). *Acta Metall. Mater.* **39**, 1603–1615.

Kronberg, M. L. & Wilson, F. H. (1949). *Trans. Am. Inst. Min. Metall. Eng.* **185**, 501.
Kumar, M., King, W. E. & Schwartz, A. J. (2000). *Acta Mater.* **48**, 2081–2091.
Lu, L., Shen Y., Chen, X., Qian, L. & Lu, K. (2004). *Science*, **304**, 422–426.
Milliron, D. J., Hughes, S., Cui, Y., Manna L., Li, J., Wang, L. W. & Alivisatos, A. P. (2004). *Nature (London)*, **430**, 190–195.
Mirpuri, K. & Szpunar, J. (2004). *Micron*, **34**, 575–587.
Miyazawa, K., Iwasaki, Y., Ito, K. & Ishida, Y. (1996). *Acta Cryst.* A**52**, 787–796.
Nucci, J. A. (1997). *Appl. Phys. Lett.* **70**, 1242–1244.
Palache, C. (1932). *American Mineralogist*, **17**, 360–361. See also http://www.minsocam.org/msa/collectors_corner/arc/twindia.htm.
Pond, R. C. & Vlachavas, D. S. (1983). *Proc. R. Soc. London Ser. A*, **386**, 95–143.
Randle, V. & Brown, A. (1989). *Philos. Mag.* A**59**, 1075–1089.
Reed, B. W. & Kumar, M. (2006). *Scr. Mater.* **54**, 1029–1033.
Reed, B. W., Minich, R. W., Rudd, R. E. & Kumar, M. (2004). *Acta Cryst.* A**60**, 263–277.
Ruch, E. & Klein, D. J. (1983). *Theor. Chim. Acta*, **63**, 447–472.
Sadanaga, R. (1978). *Recent Prog. Nat. Sci. Jpn*, **3**, 143–151.
Sadanaga, R. & Ohsumi, K. (1979). *Acta Cryst.* A**35**, 115–122.
Schwartz, A. J., Kumar, M. & Brent, L. A. (2000). *Electron Backscatter Diffraction in Materials Science.* New York: Kluwer Academic/Plenum Publishers.
Sekiguchi, A., Koike, J. & Maruyama, K. (2003). *Appl. Phys. Lett.* **83**, 1962–1964.
Senechal, M. (1983). *Acta Cryst.* A**39**, 505–511.
Shao, W., Gan, Z. H., Mhasisalkar, S. G., Chen, Z. & Li, H. (2006). *Thin Solid Films*, **504**, 298–301.
Shubnikov, A. V. & Koptsik, V. A. (1974). *Symmetry in Science and Art.* New York: Plenum Press.
Stewart, I. (2004). *Nature (London)*, **427**, 601–604.
Sutton, A. P. & Balluffi, R. W. (1995). *Interfaces in Crystalline Materials*, pp. 684–688. Oxford University Press.
Wadhawan, V. K. (1997). *Acta Cryst.* A**53**, 546–555.
Watanabe, T. (1985). *J. Phys.* **C4**, 555–566.
Wei, H. L., Huang, H., Woo, C. H., Zheng, R. K, Wen, G. H. & Zhang, X. X. (2002). *Appl. Phys. Lett.* **80**, 2290–2292.
Weinstein, A. (1996). *Notices Am. Math. Soc.* **43**, 744–752. See also http://en.wikipedia.org/wiki/Groupoid.
Wilbrandt, P. J. (1980). *Phys. Status Solidi A*, **61**, 411–418.